Optical~~,~~ **and** chemical properties and oxidative potential of aqueous-phase products from OH and $^3C^*$-initiated ~~photolysis~~photooxidation of eugenol

Xudong Li[1], Ye Tao[1], Longwei Zhu[1], Shuaishuai Ma[1], Shipeng Luo[1], Zhuzi Zhao[1], Ning Sun[1], Xinlei Ge[2,*], Zhaolian Ye[1,*]

[1]College of Chemistry and Environmental Engineering, Jiangsu University of Technology, Changzhou 213001, China

[2]Jiangsu Key Laboratory of Atmospheric Environment Monitoring and Pollution Control, Collaborative Innovation Center of Atmospheric Environment and Equipment Technology, School of Environmental Sciences and Engineering, Nanjing University of Information Science and Technology, Nanjing 210044, China

*Correspondence: Zhaolian Ye (bess_ye@jsut.edu.cn) and Xinlei Ge (caxinra@163.com)

Abstract: Aqueous reactions may turn precursors into light-absorbing and toxic products, leading to air quality deterioration and adverse health effects~~, etc~~. In this study, we investigated comprehensively eugenol photooxidation (a representative biomass burning emitted, highly substituted phenolic compound) in bulk aqueous phase with direct photolysis, hydroxyl radical (OH) and an organic triplet excited state ($^3C^*$). Results show that the degradation rates of eugenol followed the order of $^3C^*$>OH >direct photolysis. ~~Quenching experiments verified that $^3C^*$ indeed played a dominant role in~~ During $^3C^*$-initiated oxidation, ~~while~~ different reactive oxygen species (ROS) including $^3C^*$, OH, $^1O_2$ and $O_2^{\bullet-}$ ~~generated~~can participate in oxidation of eugenol, quenching experiments verified $^3C^*$ was the most important ~~for~~one; while

26 during OH-initiated oxidation. ~~Photolysis~~, $O_2^{\cdot-}$ was a more important ROS than OH to

27 oxidize eugenol. The rate constants under saturated O_2, air and N_2 followed the order

28 of $k_{O_2} > k_{Air} > k_{N_2}$ for both direct photolysis and OH-initiated oxidation, but changed to

29 $k_{Air} > k_{N_2} > k_{O_2}$ for $^3C^*$-mediated oxidation. pH and dissolved oxygen (DO) levels both

30 decreased during oxidation, indicating formation of acids and the participation of DO

31 in oxidation. UV-vis light absorption spectra of the reaction products showed clear

32 absorbance enhancement in the 300-400 nm range for all three ~~cases~~sets of experiments

33 and new fluorescence at excitation/emission=250/(400-500) nm appeared, suggesting

34 the formation of new chromophores and fluorophores (brown carbon species); and these

35 species were likely attributed to humic-like substances (HULIS) as shown by the

36 increases of HULIS concentrations during oxidation. Large mass yields of products

37 (140%-197%) after 23 hours of illumination were obtained, and high oxidation degrees

38 of these products were also observed; correspondingly, a series of oxygenated

39 compounds were identified, and detailed reaction mechanism with functionalization as

40 a dominant pathway was proposed. At last, dithiothreitol (DTT) assay was applied to

41 assess oxidation potential of the reaction products, and the end products ~~in~~of all three

42 ~~photolysis conditions~~sets of experiments showed higher DDT consumption rates than

43 that of ~~the precursor~~eugenol, indicating more toxic species were produced upon

44 aqueous oxidation. Overall, our results by using eugenol as a model compound,

45 underscore the potential importance of aqueous processing of biomass burning

46 emissions in secondary organic aerosol (SOA) formation~~, as well as its impacts on~~

47 ~~particulate matter concentration and toxicity, radiative balance and climate change.~~.

49 **1 Introduction**

Photochemical reactions in atmospheric aqueous phases (cloud/fog droplets and aerosol water) can affect lifetimes of many organic species, and are an important source and pathway of secondary organic aerosol (SOA) formation (Vione et al., 2006; Zhao et al., 2012). Compared to the gasSOA formed via gas-phase photochemical oxidation, aqueous-phase SOA (aqSOA) is often more oxidized and less volatile, therefore might play an important role in haze formation, air quality and global climate change (Ervens et al., 2011; Lim et al., 2010). However, due to complexity of the aqueous reactions and influencing factors (such as precursors, oxidants, and light intensities), detailed reaction mechanism, optical property, oxidative potential (OP) and the interplay among them remain poorly understood.

Many laboratory studies have focused on aqueous-phase oxidations of low molecular weight (LMW) volatile organic compounds (VOCs), such as isoprene, terpenes (α-, β-pinene), as well as their gas-phase oxidation products (such as glyoxal, methylglyoxal, *cis*-pinonic acid and methyl vinyl ketone) (Faust et al., 2017; Herrmann, 2003; Herrmann et al., 2015; Huang et al., 2011; Lee et al., 2012; Zhang et al., 2010). Recently, aqueous oxidation of semi-/intermediate volatility VOCs (S/IVOCs), such as the phenolic compounds emitted from combustion or pyrolysis of lignin in biomass, were also extensively investigated (Barzaghi and Herrmann, 2002; Bonin et al., 2007; Chen et al., 2020; Gilardoni et al., 2016; He et al., 2019; Jiang et al., 2021; Li et al., 2014; Li et al, 2021; Ma et al., 2021; Mabato et al., 2022; Smith et al., 2014; Sun et al., 2010; Tang et al., 2020; Yang et al., 2021; Yu et al., 2016). Generally, chemical structures of precursors have profound influences on the reaction mechanisms and products, while effect of oxidants also cannot be neglected. It is evident that liquid water can contain various types of oxidants, such as singlet oxygen ($^1O_2$), nitrate radical (NO_3), hydroxyl radical (OH), and organic triplet excited states ($^3C^*$), and all can play crucial

roles in photooxidation reactions (Kaur and Anastasio, 2018; Scharko et al., 2014). Among them, OH is a ubiquitous oxidant with concentrations of 10^{-13}-10^{-12} mol·L^{-1} (Arakaki et al., 2013; Gligorovski et al., 2015; Herrmann et al., 2003). Hence, aqueous OH-induced photooxidation has been extensively studied (Chen et al., 2020; Sun et al., 2010; Yu et al., 2016). Compared to OH oxidation, ^{3}C*-initiated aqueous oxidation (photosensitized ~~reaction~~reactions) has also attracted attentions in recent years (Ma et al., 2021; Wang et al., 2021). Several classes of organic compounds in ambient air, including non-phenolic aromatic carbonyls, quinones, aromatic ketones and nitrogen-containing heterocyclic compounds, can form ^{3}C* after absorbing light (Alegría et al., 1999; Kaur et al., 2019; Nau and Scaiano, 1996; Rossignol et al., 2014; Chen et al., 2018). These compounds are termed ~~as~~ photosensitizers. ^{3}C* is capable of reacting with O_2 to produce singlet oxygen ($^1O_2$) and superoxide radicals ($O_2^{\bullet-}$). Various reactive oxygen species (ROS) can be generated and affect greatly the ^{3}C*-initiated aqueous-phase reactions. Despite some studies demonstrating importance of ROS in photochemical process (Ma et al, 2021; Wang et al., 2020; Wang et al., 2021~~; Wu et al., 2021~~), our current understanding on ^{3}C*-initiated oxidation is still limited.

Excitation-emission matrix (EEM) fluorescence spectroscopy, as a low-cost, rapid, non-destructive and high-sensitivity technique, can offer detailed information on chromophores hence has been widely employed for studies of aquatic dissolved organic matter (Aryal et al., 2015). Nevertheless, it has not been extensively used in atmospheric aerosol research (Mladenov et al., 2011). Prior studies have investigated the relationship between the fluorescence components and chemical structures of atmospheric aerosols by using high-resolution aerosol mass spectrometry (AMS) and EEM fluorescence spectroscopy (Chen et al., 2016a; Chen et al., 2016b). An earlier report from Chang and Thompson (2010) found fluorescence spectra of aqueous-phase

100   reaction products of phenolic compounds, which had some similarities with those of

101   humic-like substances (HULIS), and Tang et al. (2020) reported that aqueous

102   photooxidation of vanillic acid could be a potential source of HULIS. Chang and

103   Thompson (2010) also showed that light-absorbing and fluorescent substances

104   generally had large conjugated moieties (i.e., quinones, HULIS, polycyclic aromatic

105   hydrocarbons (PAHs)), which can damage human body (Dou et al., 2015; McWhinney

106   et al., 2013). HULIS are considered as an important contributor to induce oxidative

107   stress since they can serve as electron carriers to catalyze ROS formation (Dou et al.,

108   2015; Ma et al., 2019; Huo et al., 2021; Xu et al., 2020), causing adverse health effects.

109   Dithiothreitol (DTT) assay (Alam et al., 2013; Verma et al., ~~2015a~~2015), as a non-

110   cellular method, was widely employed to determine oxidation activity and OP of

111   atmospheric PM (Chen et al., 2019; Cho et al., 2005) for the evaluation of its health

112   effects. Some other works (Fang et al., 2016; McWhinney et al., 2013; Verma et al.,

113   2015; Zhang et al., 2022) focused on the link between chemical

114   ~~composition~~components and OP in PM, and confirmed that several kinds of compounds,

115   such as quinones, HULIS and transition metals usually had strong DTT activities.

116   However, DTT method is rarely used to evaluate the OP of aqueous-phase oxidation

117   products previously (Ou et al., 2021).

118   In the present work, we chose eugenol (ally guaiacol) as a model compound to

119   conduct aqueous oxidation experiment. As a representative methoxyphenol emitted

120   from biomass burning (BB) (Hawthorne et al., 1989; Simpson et al., 2005), it was

121   widely detected in atmospheric particles. For instance, concentration and emission

122   factor of this compound from beech wood burning were 0.032 $\mu g/m^3$ and 1.534 $\mu g/g$,

123   which were twice those of guaiacol (0.016 $\mu g/m^3$ and 0.762 $\mu g/g$) (Bari et al., 2009).

124   Eugenol is a semivolatile aromatic compound with a moderate water-solubility (2.46

125 g/L at 298 K) too.). Chemical characteristics of aqueous reaction products under direct

126 photolysis (without oxidant) and oxidations by OH radicals and ^{3}C* radicalstriplet

127 states, were comprehensively elucidated by a suite of analytical techniques including

128 high-performance liquid chromatography (HPLC), ultraviolet and visible (UV-Vis)

129 spectrophotometry, gas chromatography mass spectrometry (GC-MS), EEM and soot

130 particle aerosol mass spectrometry (SP-AMS). The relative importance of various ROS

131 species to eugenol degradation was explored. Moreover, light absorption, fluorescent

132 and oxidative properties of the aqueous oxidation products were also investigated.

2 Materials and methods

2.1 Chemicals and reagents

135 Eugenol (99%), tert-butanol (TBA, 99%), 3,4-dimethoxybenzaldehyde (DMB,

136 99%), para-benzoquinone (*p*-BQ, 99%), dithiothreitol (99%) and 5,5′-dithiobis-2-

137 nitrobenzoic acid (DTNB, 99%), 2-nitro-5-thiobenzoic (99%), 5,5-dimethyl-1-

138 pyrroline N-oxide (DMPO), 2,2,6,6-tetramethylpiperidine (TEMP) were all purchased

139 from Sigma-Aldrich. Superoxide dismutase (SOD) was purchased from Bovine

140 Erythrocytes BioChemika. Dichloromethane (HPLC-MS grade, 99%), methanol

141 (HPLC-MS grade, 99%), acetonitrile (HPLC-MS grade, 98%), hydrogen peroxide

142 (H_2O_2, 35 wt %), and 2,4,6-trimethylphenol (TMP, 99%) were all obtained from

143 AcorsAcros Chemicals. Sodium azide (NaN_3, 98%) was purchased from J&K Scientific

144 Ltd. (Beijing, China). All solutions were prepared using ultrapure water (Millipore) on

145 the days of experiments.

2.2 Photochemical oxidation experiments

147   Aqueous-phase photochemical reactions were carried out in a Rayonet

148   photoreactor (model RPR-200) equipped with 16 light tubes (2 RPR-3000, 7 RPR-3500

149   and 7 RPR-4190 tubes), which was frequently used to mimic sunlight for

150   photochemical experiments and was described in details by several groups (George et

151   al., 2015; Hong et al., 2015; Huang et al., 2018; Jiang et al., 2021; Zhao et al., 2014).

152   Pyrex tubes containing sample solutions were placed in the center and received

153   radiation from surrounded lamps of all sides. To ensure mixing of the solution, a fan

154   and a magnetic stir bar were placed at the bottom of the reaction tube. The solution

155   temperature was controlled at $25\pm2°C$. The same photoreactor system and a normalized

156   distribution of photon fluxes inside the reactor have been reported elsewhere (George

157   et al., 2015), and the wavelength of light was in the range of 280~500 nm. We only

158   measured light intensity at the surface of the solution with a radiometer (Photoelectric

159   instrument factory of Everfine Corporation, Hangzhou, China), which was determined

160   to be ~2400 $\mu W/cm^2$ in the range of 290-320 nm (UVB), lower than the sunlight

161   intensity (6257.1 $\mu W/cm^2$).

162   In this work, 300 μM H_2O_2 and 15 μM DMB were added into solutions as sources

163   of OH and $^3C^*$ radicals,*, respectively. The initial concentration of eugenol was 300 μM.

164   For $^3C^*$-mediated experiments, solutions were adjusted to pH=3 by sulfuric acid in

165   order to perform experiments under optimal conditions (Ma et al., 2021; Smith et al.,

166   2014) since DMB triplet state is protonated to a more reactive form in acidic solution.

167   We conducted three sets of photolysisoxidation experiments: (A) 300 μM eugenol +

168   300 μM H_2O_2, (B) 300 μM eugenol + 15 μM DMB, and (C) 300 μM eugenol without

169   oxidants. In each series of experiments, a dark control experiment was performed

170   synchronously with a Pyrex tube wrapped by the aluminum foil. Results showed loss

171   of eugenol under dark conditions were negligible (data not shown). In addition, to

172 evaluate the roles of ROS in eugenol degradation during $^3C^*$-initiated oxidation,

173 quenching experiments by using specific scavengers to capture different ROS were

174 performed, namely TBA for OH, NaN_3 for $^1O_2$, SOD for $O_2^{\cdot-}$, and TMP for $^3C^*$,

175 respectively (Pan et al., 2020; ~~Wu~~Chen et al., ~~2021~~2020). For OH-initiated oxidation,

176 quenching experiments using p-BQ for $O_2^{\cdot-}$ (Ma et al., 2019; Raja et al., 2005), and

177 TBA for OH were conducted. For most experiments, solutions were saturated by air

178 and each experiment presented was repeated three times unless otherwise stated.

179 Average results with one standard deviation were provided. In order to further evaluate

180 the role of oxygen in photooxidation, experiments were also conducted by using

181 different saturated gases (air, N_2 and O_2).

182 **2.3 Analytical methods**

183 **2.3.1 Determination of eugenol concentrations**

184   Before and during the photochemical experiment, 2 mL of reacted solution was

185 sampled periodically and subjected to HPLC (LC-10AT, Shimadzu, Japan) analysis to

186 quantify eugenol concentration. The HPLC was equipped with an InertSustain AQ-C18

187 reverse phase column (4.6×250 mm, 5.0 μm, Shimadzu) and a UV-vis detector. The

188 mobile phase was a mixture of acetonitrile/H_2O (v/v: 60/40) at a flow rate of 0.6

189 mL/min, and the detection wavelength was 280 nm. The first-order kinetic rate constant

190 of eugenol degradation can be obtained from the slope of plot of $-\ln(c_t/c_0)$ versus

191 reaction time as presented in Eq.(1).

192 $$\ln(c_t/c_0) = -kt \tag{1}$$

193 Where c_0 and c_t are eugenol concentrations (in μM) at the initial and reaction time

194 t, while k represents the pseudo first-order rate constant~~.~~ (in s^{-1}).

2.3.2 UV-vis and fluorescent spectra

The UV-vis light absorbance spectra of reacted solutions (placed in a 1 cm path length quartz cuvette) were measured by using an UV-vis spectrophotometer (Specord 210 plus, Analytik Jena., Germany). The instrument has a dual-beam optical system with tungsten and deuterium lamps as light sources. A reference absorption spectrum of ultrapure water was carried out in the same cuvette prior to sample analysis for baseline correction.

Immediately after the UV-Vis measurement, the cuvette was transferred to a three-dimensional EEM fluorescence spectrometer (FluoroMax Plus,HORIBA Scientific). The ranges of wavelength varied from 200 to 450 nm for excitation wavelengths (Ex) and from 290 to 650 nm for emission wavelength (Em). Intervals of the excitation and emission wavelengths were 5 nm and 2 nm, respectively. The reported absorbance and EEM spectra here are averages of the results from experiments in triplicate.

2.3.3 Determination of HULIS concentrations

Solid phase extraction (SPE) cartridges (CNW Poly-Sery HLB, ~~60mg~~60 mg/cartridge) were used to isolate HULIS from the reaction products. The SPE cartridge was first rinsed with 1 mL ultrapure water and 3 mL methanol prior to extraction. The solution was acidified to pH ~2 using HCl and loaded on an SPE cartridge, which was rinsed with 1 mL ultrapure water again. Next, 3 mL methanol/ammonia (98:2, v/v) mixture was added into the SPE cartridge to elute HULIS, and the solution was ~~blew~~blown to full dryness with high purity N_2, followed by dilution with ultrapure water to 25 mL for quantification of HULIS using the HPLC coupled with an evaporative light scattering detector (ELSD3000). Recovery efficiency

of the HULIS standard, Suwanne River Fulvic Acid (SRFA), was 75-80% with the

standard deviation of reproducibility less than 5%. More details have been described

elsewhere (Tao et al., 2021).

2.3.4 Oxidative ~~potentials (OPs~~potential (OP) based on DTT assay

The ~~OPs~~OP of reaction products ~~were~~was determined by the DTT method (Cho et

al., 2005; Lin and Yu, 2019) with slight improvements. Briefly, 1.2 mL sample solution

was transferred into a 10 mL glass tube, then 6 mL phosphate buffer (0.1 M, pH 7.4)

and 300 µL of 2.5 mM DTT were added and mixed thoroughly. The DTT mixed

solution was placed in a 37°C water bath for incubation. Over the course of reactions

that lasted for 150 minutes, 1 mL aliquot of DTT mixture was taken every 30 minutes,

and 100 µL of 5 mM DTNB (prepared in 0.1 mM phosphate buffer) was added and

loaded in a centrifuge tube. Next, reactions between DTNB and DTT produced bright

yellow TNB, which was quantified by the UV-Vis spectrometer within 30 minutes.

Finally, we measured the light absorbance (A_t) at 412 nm ~~at time t~~ to indirectly quantify

the remaining DTT. Another 1.2 mL ultrapure water instead of sample solution was

treated in the same way and the absorbance was denoted as A as the blank value. A_0

represents the initial light absorbance value. Thus, DTT concentration consumed by the

sample solution (M_{DTT}, µM) and that by the blank solution (M_{DTT0}, µM) can be

calculated according to Eq.(2) and Eq.(3), respectively.

$$M_{DTT} = \frac{A_0 - A_t}{A_0} \times C_{DTT0} \tag{2}$$

$$M_{DTT0} = \frac{A_0 - A}{A_0} \times C_{DTT0} \tag{3}$$

Here, C_{DTT0} was the initial DTT concentration in sample solution (100 µM in this

work). DTT consumption rates (R_{DTT} and R_{DTT0}) were then obtained from the slopes of

plots of M_{DTT} and M_{DTT0} versus incubation times. Experiments of blanks and samples

were typically run in a triplicate. The reproducibility of the whole analysis showed that the relative standard deviation of DTT consumption rate was 3-4%.

2.3.5 ~~Products~~Product analysis by GC-MS

Reacted solution (about 30 mL) was extracted with 10 mL dichloromethane twice. The extract was concentrated into 1 mL by blowing N_2 gently, subsequently transferred to a 2 mL vial, and analyzed by a GC-MS (7890A GC/5975C MS, Agilent) with a DB-5ms capillary column (30 m×0.25 mm×0.5 μm). The operational conditions were set as follows: injector was at 200℃; ion source was at 230 ℃; column oven temperature was programmed to be held at 35℃ for 4 minutes, then ramped to 250 ℃ at a rate of 20℃/minute and held for 10 minutes. The recovery efficiency, method detection limits and quality assurance/quality control have been described in our previous work (Ye et al., 2020).

2.3.6 SP-AMS analysis and mass yields of reaction products

An Aerodyne SP-AMS (Onasch et al., 2012) was applied to analyze the low-volatility organic products, similar to our previous work (Chen et al., 2020; Ge et al., 2017). SP-AMS data were acquired in V mode and analyzed by Squirrel v.1.56D and Pika v1.15D software. The organic fragments were classified into six groups: CH, CHO, CHN, CHO_2, CHON and HO. Elemental ratios (oxygen-to-carbon, O/C; hydrogen-to-carbon, H/C), were calculated according to the method proposed by Canagaratna et al. (2015).

Since the AMS analysis requires nebulization of sample solution into particles before determination, and quantification of organics was influenced by the atomization efficiency and carrier gas flow, ~~etc.,~~ we thus cannot use SP-AMS measured

265 concentration to quantify the mass of products directly. In this case, according to Li et

266 al. (2014), we added an internal standard (SO_4^{2-}) prior to AMS analysis, and the mass

267 ratio of particle-phase organics to SO_4^{2-} ($\Delta Org/SO_4^{2-}$) can be used to calculate the mass

268 concentration of products. Furthermore, the mass yield of aqueous-oxidation products

269 ($Y_{products}$, %), which is the mass of products generated per unit mass of precursor

270 consumed, can be calculated ~~as~~according to Eq. (4).

$$Y_{products}(\%)=\frac{(\Delta Org/SO_4^{2-})[SO_4^{2-}]_0}{C_0 M \eta} \times 100\% \tag{4}$$

272 Where $[SO_4^{2-}]_0$ is the SO_4^{2-} concentration (here 7.27 mg~~-~~/L^{-1}), C_0 is the initial eugenol

273 concentration (in mmol/L), M is MW of the precursor (164 g/mol for eugenol) , and η

274 is the degraded fraction of eugenol.

3 Results and discussion

3.1 Kinetics of aqueous photooxidation

277   Figure 1 shows unreacted eugenol concentrations (c_t) and the negative logarithm

278 of c_t/c_0 (-ln(c_t/c_0)) as a function of reaction time, respectively. The pseudo first-order

279 rate constants (k) obtained by Eq.(1) were also presented. As described in Fig. 1a,

280 eugenol concentration decreased to be <20% of the initial concentration in 3 hours,

281 suggesting ~~photolysis~~photooxidation was fast under all three reaction conditions. In the

282 presence of $^3C^*$, eugenol was degraded nearly 100% after 3 hours. Previous study (Chen

283 et al., 2020) on $^3C^*$-initiated 4-ethylguaiacol oxidation reports a time of 21 hours for a

284 complete degradation. Apart from difference of precursors, different light irradiation

285 spectra and stronger energy of light in this work than the previous work might be

286 responsible for the fast loss of eugenol. The bond dissociation energies (BDEs) are 340

287 kJ/mol for OH, 374 kJ/mol for C-H in -CH$_3$ group, 345 kJ/mol for C=C bond, and 403

288 kJ/mol for C-H in -OCH$_3$ group, respectively (Herrmann et al., 2003; He et al., 2019).

289 ~~The lowest BDE was found for the O-H bond and C=C bond.~~ Due to influences of steric

290 hindrance and intramolecular hydrogen bonding, the H-abstraction from OH group

291 might not be favorable and the most probable H-abstraction might take place in C=C

292 of the allyl group. As a result, breakage of C=C into C-C at the allyl group can lead to

293 the formation of 2-methoxy-4-propyl-phenol (Section 3.6.1). When photon energy is

294 higher than the BDE, chemical bonds can break, leading to decomposition of

295 compounds and possibly further mineralization. The ~~energies~~energy of ~~photons~~

296 ~~at~~photon of 300 ~~and 350~~ nm ~~are~~is 412 kJ/mol~~, and~~ and can break all major bonds in

297 eugenol, while the energy of 350 nm is 353 kJ/mol, ~~higher than~~being able to break some

298 of the ~~weakest BDE~~bonds in eugenol~~, therefore it~~ as well. Overall, eugenol can be easily

299 decomposed after absorbing the ~~photon~~photons.

300   As shown in Fig. 1b, the first-order rate constants were 2.43×10^{-4} s^{-1}, 2.73×10^{-4} s^{-1}

301 ^{1}, and 5.75×10^{-4} s^{-1} for direct photolysis and photooxidations by OH and ^{3}C*,

302 respectively. ^{3}C*-initiated photooxidation was quicker than that attacked by OH, likely

303 due to combined contributions from reactions with ^{1}O$_2$, O$_2^{\bullet-}$ and OH (Section 3.2).

304 Similar results were found for aqueous phase reactions of three phenols against OH and

305 ^{3}C* by Yu et al. (2016) (Note the initial concentrations of H$_2$O$_2$ and DMB were 100 μM

306 and 5 μM, respectively, with the same ratio as 300 μM H$_2$O$_2$ to 15 μM DMB in this

307 work)
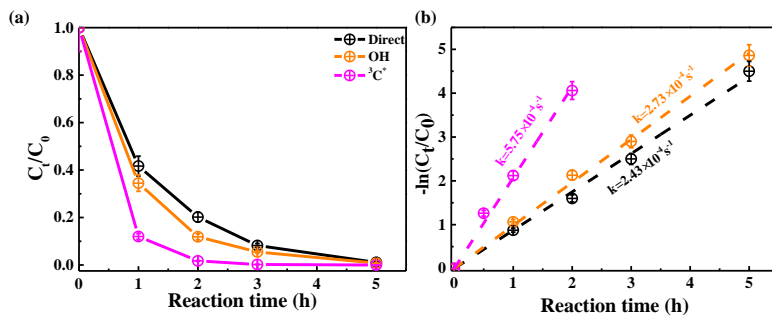
308

309 **Figure 1.** Aqueous-phase eugenol decay kinetic curves (a) and ~~regressed~~ first-order rate constants

310 (b) obtained based on Equation 1 under ~~three conditions~~direct photolysis, OH-initiated oxidation

311 and ^{3}C*-initiated oxidation. Error bar represents one standard deviation from the measurements in

312 triplicate.

313 **3.2 Relative importance of ROS in photooxidation**

314 **3.2.1 Quenching experiments in ^{3}C*-initiated photooxidation**

315   Relative importance of different ROS in photooxidation can be investigated by

316 addition of ~~radical~~ scavengers/quenchers, and then be evaluated based on the different

317 degradation efficiencies of eugenol in absence and presence of the corresponding ROS

318 quenchers. For each quencher, we conducted several gradient experiments with varying

319 molar ratios of eugenol to quencher. The ratios were 0.075:1, 0.15:1, 0.3:1, 0.75:1, 1.5:1

320 for quenchers of NaN$_3$, TMP and TBA, and 1.2:1, 1.6:1, 2.5:1, 5:1, 10:1 for SOD, which

321 were all within the typical ranges of ROS quenching experiments reported previously

322 (Zhou et al., 2018). Excess concentrations of quenchers have been added repeatedly to

323 ensure the complete reactions between ~~radicals~~ROS and scavengers. Figure 2 displays

324 the impacts of quenchers on eugenol degradation. All rate constants (k) with quenchers

325 were lower than those of the quencher-free solutions. The optimum molar ratio of

326 eugenol to quencher was ~~chosen when~~selected such that the ~~inhibition degree of~~

带格式的: 两端对齐

eugenol degradation ~~unchanged~~did not change with the increase of added quencher

(Wang et al., 2021). For example, along with the decrease of molar ratios of eugenol to

NaN$_3$ from 1.5:1 to 0.075:1, the ~~inhibitory degree~~variation of eugenol degradation was

stabilized at the ratio of 0.15:1, indicating that $^1O_2$ has been completely quenched at

this ratio, therefore a molar ratio of 0.15:1 for NaN$_3$ was optimal, since excess

scavenger may generate other products that interfere the existing reactions.

~~Similarly~~Finally, the optimal molar ratios of eugenol to quenchers of TBA, NaN$_3$, TMP

and SOD, were determined to be 1.5, 0.15, 0.075 and 2.5, respectively. Table 1 and Fig.

S1 compared the rate constants determined under the ratios above and they were in an

order of TMP<NaN$_3$<SOD<TBA, suggesting relative importance of generated ROS to

eugenol degradation was in the order of $^3C^*>{}^1O_2>O_2{}^{\bullet-}>OH$. This result suggests that

$^3C^*$ plays a major role among all ROS in the photooxidation. Previously, Laurentiis et

al. (2013) reported that 4-carboxybenzophenone (70 μM) could act as $^3C^*$ and the

photosensitized degradation was more effective than oxidants such as OH, O$_3$~~, etc.;~~:

Misovich et al. (2021) investigated the aqueous DMB-photosensitized reaction (5 μM,

same as ~~it~~in this study) also demonstrated that $^3C^*$ was the greatest contributor to phenol

or guaiacyl acetone degradation, followed by $^1O_2$, while both OH and $^1O_2$ contributions

were relatively minor.

~~We~~To further assess the relative importance of different ROS, we propose to use

the following Eq.(5) ~~to roughly assess the contribution of~~ for a ~~certain ROS (Ct$_{ROS}$) to~~

~~eugenol degradation~~rough estimation:

$$\text{~~Ct}_{ROS}\text{=}k_{ROS}\text{/k=(~~}Red_{ROS} \text{ (in \%)}= (k-k_{quencher})/k \times 100\%$$

(5)

Here ~~k$_{ROS}$~~k (in s^{-1}) is the ~~rate constant contributed by the ROS, which is defined as the~~

~~difference between the~~ original rate constant ~~in~~of $^3C^*$-initiated oxidation (~~k~~or OH-

initiated oxidation in Section 3.2.2) and $k_{quencher}$ (in s^{-1}) is the rate constant ~~–~~after the

target ROS has been completely scavenged by its ~~corresponding~~ quencher ~~($k_{quencher}$)~~. k

and $k_{quencher}$ in fact refer to those reported in Fig. S1b. Red_{ROS} then refers to the

percentages of reduction due to addition of quencher for a ROS.

According to Eq.(5), ~~Ct_{3C}~~Red_{3C^*} was calculated to be ~~0.857, therefore contribution~~

~~of $^3C^*$ was estimated to be as high as~~ 85.7%. Similarly, the ~~contributions~~values of $^1O_2$,

$O_2^{\bullet-}$ and OH were 80.5%, 61.4% and 53.9%, respectively. ~~The total contribution of the~~

~~four ROS largely exceeded 100%. This~~Note Red_{ROS} only reflects the relative important

of ROS and it does not corresponds to the exact contribution of that ROS in eugenol

degradation without quenchers. The reason is that although the addition of a ROS

scavenger can ~~be explained~~eliminate oxidation by ~~the fact that~~this ROS ~~scavengers can~~

~~actually~~, but it also significantly ~~interrupt~~interrupts the ~~radical~~original chain reactions

as compared to those in the absence of ~~scavengers. For instance, addition of TMP not~~

~~only scavenges $^3C^*$, but also inhibits generation of $^1O_2$, $O_2^{\bullet-}$, etc. These findings suggest~~

~~that we cannot directly precisely quantify the contribution of a ROS just on the basis of~~

~~its scavenging efficiency, therefore the contributions calculated from Eq.(5) can only~~

~~be used to compare the relative importance of different ROS. One~~the scavenger, and

reactions with other ROS might be enhanced. In this regard, the sum of the four Red_{ROS}

values may exceed 100%. Therefore, one should be cautious to ~~apply quenching~~

~~approach to quantify the role of ROS in complex reaction system~~use Red_{ROS} as a precise

quantification of the ROS contribution in aqueous oxidation. Determination of ROS

concentrations during oxidation should be instead be an effective way to elucidate the

role of ROS. ~~Therefore~~Here, we tried to detect in-situ generated OH, $O_2^{\bullet-}$ and $^1O_2$ during

photochemical reactions using a micro electron spin resonance (ESR) spectrometer

(Bruker Magnettech, Berlin, Germany) with DMPO as the spin trap to form stable

377 DMPO-OH or DMPO-O$_2^{\bullet-}$, with TEMP to capture $^1O_2$ to produce TEMP-$^1O_2$ spin-

378 adduct (TEMPO). The radicals can be identified and quantified by the peak patterns in

379 ESR spectra, such as the quarter line with a height ratio of 1:2:2:1 for DMPO-OH,

380 1:1:1:1 for DMPO-O$_2^{\bullet-}$ and 1:1:1 for TEMP-$^1O_2$ (Guo et al., 2021). Unfortunately, OH

381 radical cannot be detected since its ~~concentrations~~concentration might be lower than

382 the detection limit of the instrument (Fig. S2, ESR spectra of OH). In contrast, we were

383 able to detect ~~higher~~high concentrations of $^3C^*$ and found the intensity of TEMP-$^1O_2$

384 signal reached its maximum at 30 minutes, then decreased slowly (Fig. S2, ESR spectra

385 of $^1O_2$). Combining the ~~greatest inhibitive~~great quenching effect of TMP with high $^1O_2$

386 concentration from ESR method, we can conclude that $^3C^*$ and $^1O_2$ play relatively

387 important roles in eugenol photooxidation.
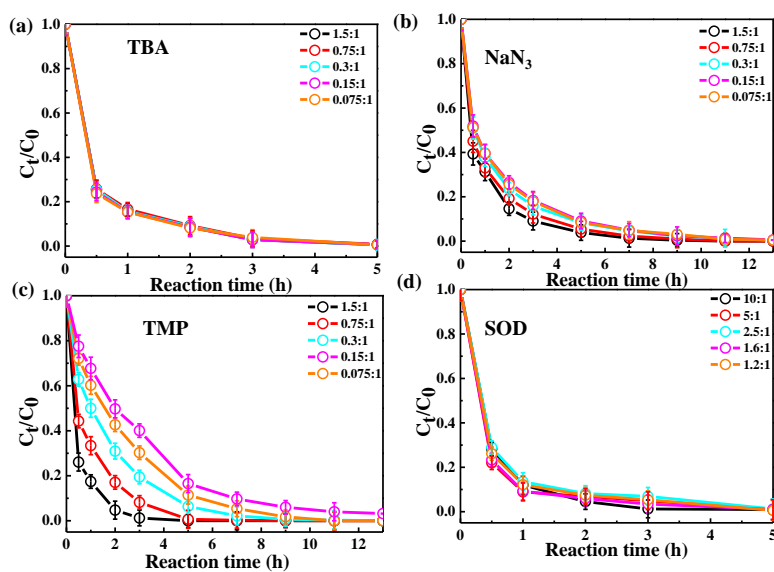
388

389 **Figure 2.** Ratio of unreacted eugenol concentration to its initial concentration (C_t/C_0) at different

390 molar ratios of eugenol to quencher, as a function of reaction time: (a) TBA, (b) NaN$_3$, (c) TMP and

391 (d) SOD.

392

3.2.2 Quenching experiments in OH-initiated photooxidation

To examine the contributions of ROS to eugenol degradation for OH-initiated oxidation, TBA and p-BQ as trapping agents were added. Similar to $^3C^*$-initiated oxidation, several gradient experiments with varying molar ratios of eugenol to quenchers were conducted. The ratios were set as 6.5:1, 3.2:1, 1.6:1, 1.1:1 and 0.8:1 for p-BQ and 3.0:1, 1.5:1, 0.75:1, 0.3:1 and 0.15:1 for TBA. According to Fig. S3, molar ratio only had a slight influence on eugenol degradation, although degradation can be inhibited effectively by quenchers. Thus, we determined the appropriate molar ratios of 0.8 and 0.75 for p-BQ and TBA, respectively, as excess scavengers might influence the chemical reactions.

Variations of the rate constants for the aforementioned quenching experiments were determined, in comparison with those conducted without quenchers, and the results are listed in Table 1 and presented in Fig. S4. For TBA quenching tests, the rate constant decreased by 18.7% (from 2.73×10^{-4} s^{-1} to 2.22×10^{-4} s^{-1}), showing that OH radical played a certain role in eugenol photooxidation. Since H_2O_2 was mainly photolyzed at wavelength <300 nm to generate OH radical, irradiation above 300 nm did not affect the reaction significantly. The p-BQ could quench $O_2^{\cdot-}$, further suppressing the generation of other ROS (e.g., $\cdot HO_2$), therefore the rate constant decreased the most (from 2.73×10^{-4} s^{-1} to 1.20×10^{-4} s^{-1}), suggesting $O_2^{\cdot-}$ was important for eugenol photooxidation. This hypothesis could be further confirmed by the decline of rate constant under N_2-saturated solution (Section 3.2.3). However, it was difficult to detect both OH and $O_2^{\cdot-}$ directly due to their relatively short lifetimes and low concentrations via ESR in this work.

417 **Table 1.** The first-order rate constants of eugenol in the presence of various scavengers. The initial

418 conditions were as follows: 300 μM eugenol; molar ratios of eugenol to quenchers TBA, NaN$_3$,

419 TMP and SOD, of 1.5, 0.15, 0.075 and 2.5, respectively; molar ratios of eugenol to quenchers p-BQ

420 and TBA of 0.8 and 0.75, respectively.

^{3}C*-initiated quenching experiments			
Quenchers	ROS	Reaction rate constant k (s^{-1})	Pearson's R^2
no quencher	-	5.75×10^{-4}	0.996
TBA	OH	2.65×10^{-4}	0.999
SOD	O$_2^{\cdot-}$	2.22×10^{-4}	0.995
NaN$_3$	^{1}O$_2$	1.12×10^{-4}	0.999
TMP	^{3}C*	0.82×10^{-4}	0.999
OH-initiated quenching experiments			
Quenchers	ROS	Reaction rate constant k (s^{-1})	R^2
No quencher	-	2.73×10^{-4}	0.995
TBA	OH	2.22×10^{-4}	0.998
p-BQ	O$_2^{\cdot-}$	1.20×10^{-4}	0.995

421

3.2.3 Influences of different saturated gases

423   In order to assess the role of O$_2$ in eugenol ~~photolysis~~degradation, a series of

424 experiments were performed under both O$_2$-saturated and N$_2$-saturated conditions in

425 addition to air. N$_2$ gas was purged into reaction solution for ~30 minutes before

426 experiment to achieve the O$_2$-free condition. Figure 3 compared the changes of eugenol

427 concentrations and rate constants ~~(see insets)~~ under the three gas conditions for direct

428 photolysis, OH-initiated and ^{3}C*-initiated oxidations, respectively. The rate constants

429 followed the order of k$_{O_2}$ > k$_{Air}$ > k$_{N_2}$ under both direct photolysis and OH oxidation,

430 providing evidence in support of O$_2$ being significant for eugenol degradation. This

431 might be explained by the fact that O$_2$ can act as an electron acceptor to generate O$_2^{\cdot-}$

432 and •HO$_2$, and subsequently form H$_2$O$_2$ and OH. For direct photolysis, rate constant

433 under O$_2$-saturated condition increased 14.4% while it decreased 19.3% under N$_2$

434 saturation from that under saturated air. For OH-initiated oxidation, the difference of

rate constants under three saturated gases became more distinct.

On the contrary, rate constants followed the order of $k_{Air} > k_{N_2} > k_{O_2}$ in $^3C^*$-initiated oxidation. There are two possible explanations. On one hand, under N_2-saturated condition without oxygen, DMB would involve in reactions (R1-R4), leading to a more effective generation of $^3DMB^*$ therefore a higher degradation efficiency than under O_2-saturated condition. On the other hand, for air/O_2-saturated solutions, irradiation of DMB and eugenol would involve also reactions (R5-R8) in addition to (R1-R4), and as a result, the amount of $^3DMB^*$ ~~radical~~ decreased, due to formation of other ROS ($^1O_2$, $O_2^{•-}$, OH, etc) with relatively weak oxidative capacities. In summary, quenching of $^3DMB^*$ by ground state molecular oxygen could account for the low degradation efficiency in O_2-saturated condition.

$$DMB + h\nu \rightarrow {}^1DMB^* \rightarrow {}^3DMB^* \tag{R1}$$

$$^3DMB^* \rightarrow DMB \tag{R2}$$

$$^3DMB^* \rightarrow Products \tag{R3}$$

$$^3DMB^* + {}^1DMB^* \rightarrow DMB^{•+/•-}(DMB^{•+}+DMB^{•-}) \tag{R4}$$

$$^3DMB^* + O_2 \rightarrow DMB + {}^1O_2 \tag{R5}$$

$$DMB^{•-} + O_2 \rightarrow \cdot DOM^+ + O_2^{•-} \tag{R6}$$

$$O_2^{•-} + 2H^+ \rightarrow H_2O_2 + O_2 \tag{R7}$$
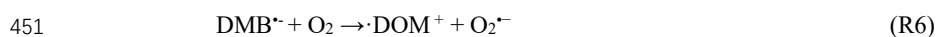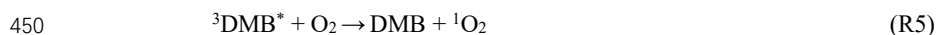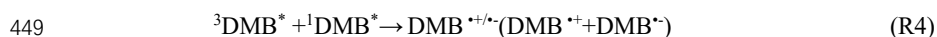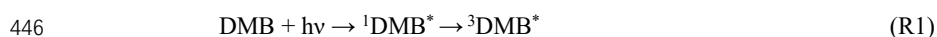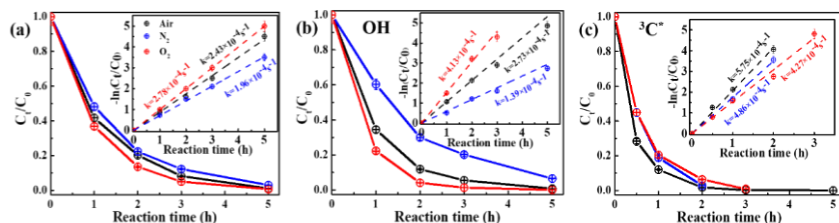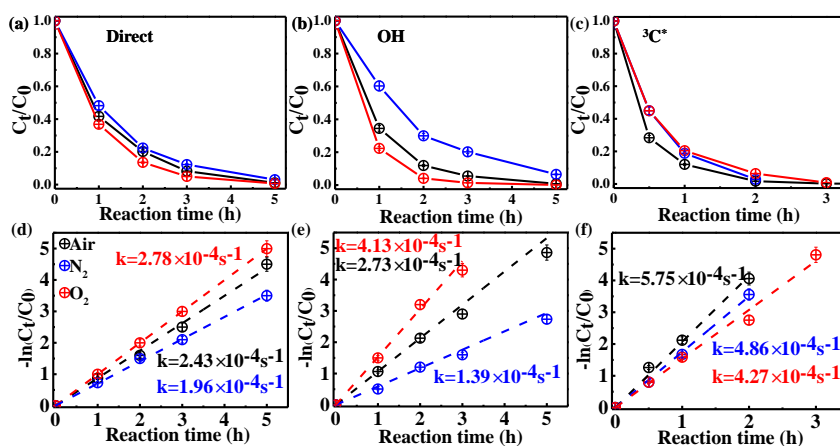
$$H_2O_2 \rightarrow 2OH \tag{R8}$$

Figure 3. Ratio of unreacted eugenol concentration to its initial concentration (C_t/C_0) as a function of reaction time at different saturated gases under (a) direct photolysis (b) OH-initiated oxidation and (c) $^3C^*$-initiated oxidation. ~~The insets in (a-c) show the corresponding rate~~Rate constants ~~of~~ of (a-c) are presented in (d-f) correspondingly.

3.2.4 Variations of pH and dissolved oxygen

The initial pH values of reaction solutions for direct photolysis and OH-initiated oxidation were unadjusted, while ~~those~~that for the $^3C^*$-oxidation was adjusted to 3. The variation of solution pH is presented in Fig. 4a. The pH values decreased ~~dramatically~~quickly at the beginning of illumination (from 7.4 to ~5.0 in the first 1 hour) then tended to be flat for both direct photolysis and OH-initiated oxidation. However,

468 little change of pH (less than 0.1 unit) was observed for the $^3C^*$-initiated photooxidation

469 throughout the oxidation, ~~which can be~~ likely ~~ascribing~~ascribed to its low initial pH of

470 3. ~~Note a small amount of acids can change solution pH significantly when original pH~~

471 ~~is high, but cannot change pH remarkably when~~Since the ~~original~~ solution pH was ~~low.~~

472 ~~Therefore,~~acidic (pH=3), we cannot rule out formation of acidic products (such as

473 organic acids) during $^3C^*$-initiated oxidation as during direct photolysis and OH-

474 initiated oxidation.

475 As discussed in Section 3.2.3, oxygen can take part in photochemical reaction to

476 form ROS, which may in turn destroy the structure of precursor. Here we measured the

477 oxygen consumption during oxidation through determination of dissolved oxygen (DO)

478 contents by a dissolved oxygen meter (Seven2Go Pro S9, Zurich, Switzerland). DO was

479 consumed mainly at the first 1 hour and remained stable afterwards ~~with the increase~~

480 ~~of reaction time~~ (Figs. 4b-c and Fig. S5). The amounts of consumed DO followed the

481 order of $^3C^*$>OH>direct photolysis. The maximum consumed DO was found in $^3C^*$-

482 initiated oxidation, which ~~can~~might be explained by the ~~transfer~~consumption of

483 ~~electrons from~~O_2 that reacts with $^3C^*$ ~~to O_2 to~~ form $^1O_2$~~, a major contributor to eugenol~~

484 ~~degradation.~~ (R5). Obviously, a steady-state DO level was reached when the

485 consumption rate was equal to the diffusion of O_2 into the solution (Pan et al., 2020).

486 Overall, these results re-emphasize that O_2 can influence eugenol degradation and

487 ~~radical~~chemical transformation via induction of radical chain reactions.

488
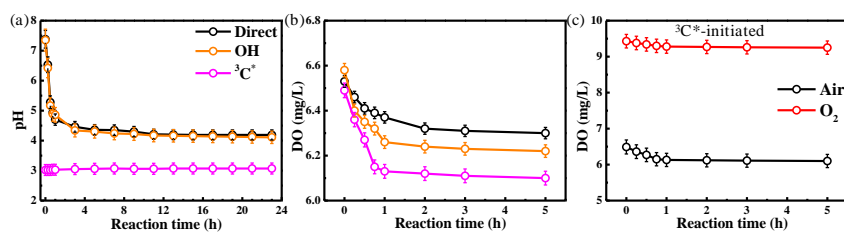
Figure 4. (a) pH values and (b) ~~dissolve~~dissolved oxygen (DO) contents against reaction time under ~~three~~direct photolysis ~~conditions~~, OH-initiated oxidation, ^{3}C*-initiated oxidation, and (c) DO contents during ^{3}C*-initiated oxidation under air or O_2-saturated conditions.

带格式的: 两端对齐

3.3 Optical properties of reaction products

3.3.1 Light-absorbing properties

The UV-vis light absorption spectra of the solutions at different reaction times are presented in Fig. 5. The light absorption by eugenol itself mainly occurs in the range of 260-300 nm (n→π* electronic transition, 270-350 nm), which overlaps with the major photon fluxes (280 and 500 nm) of our lamp for ~~photooxidations.~~photooxidation. Therefore, we can clearly observe that the characteristic absorption peak at 280 nm of precursor decreased with the propagation of direct photolysis (Fig. 5a), similar to that in OH-initiated photooxidation (Fig. 5b). However, the reaction was quick in the presence of ^{3}C*, and the characteristic absorption peak at 280 nm after 3 hours of illumination almost disappeared, suggesting nearly a complete loss of eugenol, consistent with the results in Section 3.1 that more than 99% eugenol was degraded in 3 hours. Additionally, there was an obvious absorption enhancement at longer wavelengths (300-400 nm) during the photooxidation, whereas eugenol itself did not absorb light in this range, indicating some light-absorbing products (e.g., brown carbon (BrC) species) were generated. Aqueous photooxidation of some phenolic compounds (e.g., vanillic acid) also presented long-wavelength (300-400nm) light absorbance, with intensity increasing with illumination time (Tang et al, 2020; Zhao et al., 2015). In addition, there were some differences for light absorbance at wavelength of 300-400 nm in the three ~~cases.~~reaction conditions. For direct photolysis and OH-initiated oxidation, light absorbance increased during the first 15 hours, then remained at a plateau until 23 hours. However, for ^{3}C*-initiated oxidation, light absorbance increased

during the first 7 hours, then decreased slowly afterwards. The different shapes of UV-vis spectra between OH and $^3C^*$ photooxidations indicate formations of different products.

Compared to the light spectrum of eugenol, there were also increases of light absorbance at ~260 nm ($\pi \rightarrow \pi^*$ electronic transitions) upon aqueous ~~photolysis~~oxidation in all three reaction conditions (Fig. 5), demonstrating the generation of new substances likely with both aromatic C=C and carbonyl (C=O) functional groups (Tang et al., 2020). The enhancement at 300-400 nm may point to products with high MWs and conjugated structures~~, possibly linking with HULIS or oligomers.~~. Unfortunately, we were unable to quantify the relative contributions of individual products to the overall light absorbance between 300 to 400 nm due to lack of ~~the~~a full speciation of the products and their light absorption spectra.
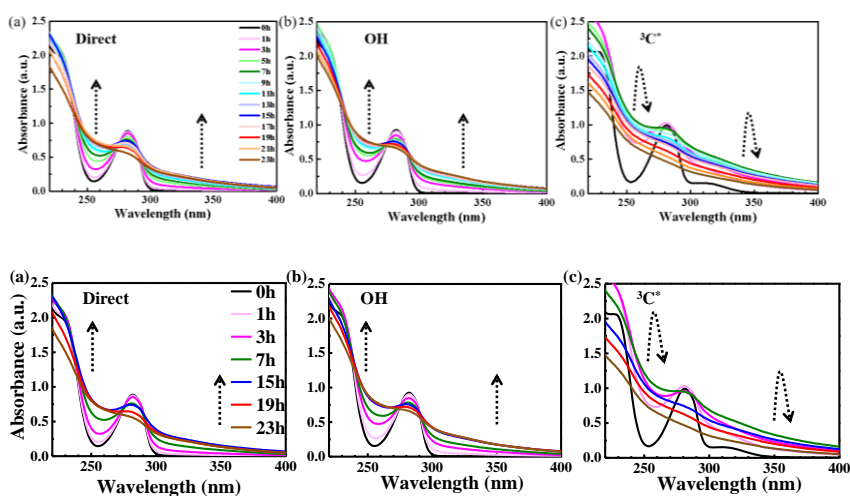
Figure 5. UV–vis light absorption spectra of reacted solutions at different reaction times under (a) direct photolysis, (b) OH-initiated oxidation, and (c)$^3C^*$-initiated oxidation.

3.3.2 Fluorescence properties

The fluorescence properties of solutions before (0 hour) and during ~~photolysis~~photooxidation (3 and 7 hours) were investigated via the EEM technique, as shown in Fig. 6. For comparison, we also presented EEM profiles of pure eugenol (non-irradiated), pure DMB, and the end solutions (23 hours) of direct photolysis and OH-initiated oxidation in Fig. S6. The peaks at Excitation/Emission (Ex/Em)=275/313 nm can be attributed to fluorescence of the phenolic structure of parent substance (eugenol here), as suggested by Laurentiis et al. (2013). As shown in both Fig. 6 and Fig. S6, the fluorescence intensity decreased after ~~photolysis~~oxidation due to eugenol decay, and the reduction was very fast for $^3C^*$-initiated oxidation. This finding matches with the fast ~~photolysis~~degradation and large rate constant for $^3C^*$-initiated oxidation. The EEM plots for direct photolysis and OH-initiated oxidation had similar contour patterns as shown in Figs. 6a and b, although EEM profiles changed significantly with irradiation time. We also observed distinct fluorescent peaks at Ex/Em=235/(400-500) nm, indicating that illumination can cause a red shift in fluorescence emission wavelength. As suggested by Chang et al. (2010), fluorophores at Ex/Em=240/400 nm are linked with aromatic structures and condensed saturated bonds including polycyclic aromatic hydrocarbons. Another work (Li et al., 2021) showed that red shift in the fluorescence spectra was usually related to an increase in the size of ring system and an increase in the degree of conjugation. Previous studies (Chen et al., 2016a; Chen et al., 2019~~; Laurentiis et al., 2013; Wu et al., 2019~~) have reported that fluorescent compounds with emission wavelength at 400-500 nm ~~may be highly oxygenated species such as~~were likely linked with HULIS. Additionally, HULIS have two typical fluorescent peaks in EEM profile at Ex/Em=(200-300)/(400-500) nm and Ex/Em=350/(400-500) nm with the former one having a higher intensity (Graber and Rudich, 2006; Laurentiis et al., 2013; Vione et al., 2019~~; Wu et al., 2021~~). There was also evidence that direct photolysis

of tyrosine and 4-phenoxyphenol generated HULIS with new fluorescence signals at Ex/Em=(200-250)/(400-450) nm and 300/(400-450) nm (Bianco et al., 2014). In this regard, we inferred that new peak at Ex/Em=235/(400-500) nm here was likely attributed to HULIS. For the $^3C^*$-initiated ~~photolysis~~oxidation, extra fluorescent peaks at Ex/Em=(220-300)/(400-500) nm appeared in the first 1 hour (data not shown), but their intensities weakened and gradually disappeared upon prolonged ~~photolysis~~reactions (3 hours). Nevertheless, EEM results should be interpreted with ~~caveats~~caution because many ~~complicated~~ substances might contribute to absorption and emission at a certain wavelength, and it is hard to distinguish and isolate fluorescent and nonfluorescent constituents simply via the EEM technique.

Another interesting finding was that a small fluorescence peak appeared at Ex/Em=(300-350)/(300-350) nm in some of the EEM profiles. Specifically, it appeared earlier for $^3C^*$-oxidation (at 3 hours) than the other two systems, yet its intensity seemed to be a bit stronger in the end solutions of direct photolysis and OH-oxidation (Fig. S6). ~~EEM fluorescence spectra of HULIS from fog water are reported to have peaks at shorter excitation and emission wavelengths than those of terrestrial fulvic acids (Graber and Rudich, 2006).~~ Moreover, as suggested by Leenheer and Croue (2003), fluorescence peak position of the maximum Ex/Em for HULIS with lower MWs would shift towards lower wavelengths, thus, we inferred fluorescence peak at Ex/Em=(300-350)/(300-350) nm might be in part attributed to the organic acids with ~~only~~ a few carbon atoms~~.~~ (probably C_1-C_6). Nevertheless, large uncertainties still exist in using EEM fluorescence technique to identify molecular compositions of the products due to lack of standard EEM profiles for specific compounds from aqueous phase oxidation and clearly more studies are needed in future.

581
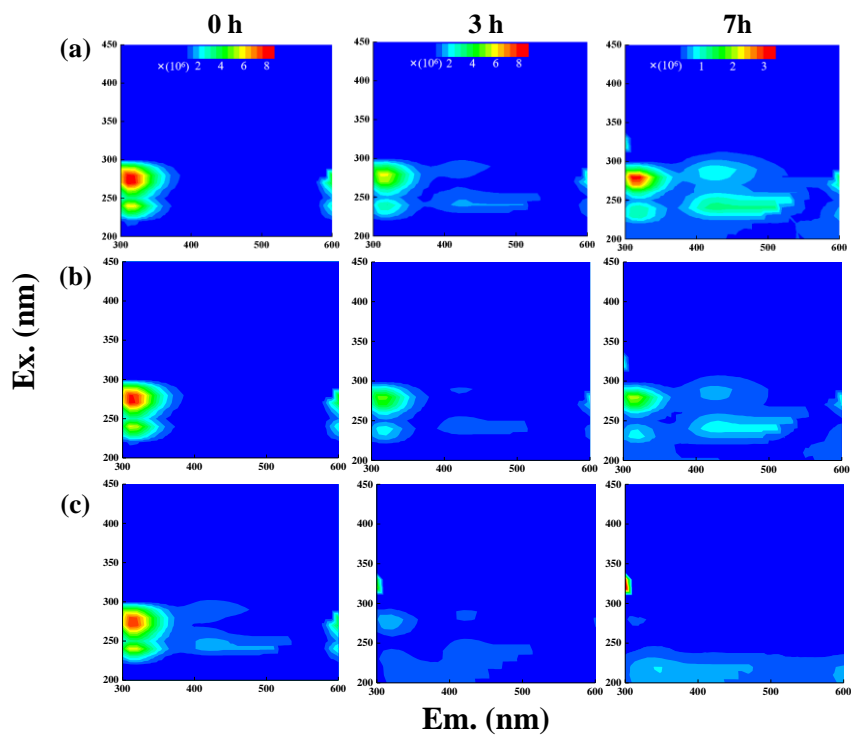
Figure 6. EEM fluorescence spectra of the initial solution (0 hour) and those at different reaction

time (3 and 7 hours) under (a) direct photolysis, (b) OH-initiated oxidation, and (c) $^3C^*$-initiated

oxidation.

585

3.4 Characteristics of HULIS

The EEM spectra revealed new prominent fluorescent peak at Ex/Em=250/(400-500) nm, which was likely owing to HULIS. HULIS can be divided into fulvic acid (water soluble at all pHs), humic acid (base soluble, acid insoluble) and humin (insoluble at all pHs). In principle, extracted HULIS in this work with polymer-based HLB SPE packing include LMW organic acids, fulvic acids and other humic substances.

Figure 7 presents the measured HULIS concentrations against the reaction time. The results show clearly that aqueous-phase eugenol oxidation is a source of HULIS, and the amount increased gradually in the first 7 hours, then remained at a similar level (about 30 mg/L) for the OH-initiated oxidation. For direct photolysis, HULIS concentration increased until 11 hours and then became steady at a level around 40 mg/L. For the $^3C^*$-oxidation, HULIS concentration increased to a maximum at 7 hours, then declined slightly afterwards. A plausible reason of such variabilities is that generated HULIS was capable of further taking part in photochemical reactions since it can act as photosensitizer. Moreover, Yu et al. (2016) characterized the products from aqueous oxidations of phenols by $^3C^*$ triplet states and OH radicals, and found both could produce oligomers and hydroxylated species but the $^3C^*$-oxidation could produce more of these compounds when 50% of the precursor was reacted. Considering the large increases of HULIS in the first 7 hours and the much faster increase of $^3C^*$-oxidation in the first 3 hours shown in Fig. 7, we postulate that HULIS species might ~~overlap with~~be some of the ~~products of~~ high MW oligomers, which can in turn contributed to fluorescence at emission of ~400 nm (Barsotti et al., 2016).

608
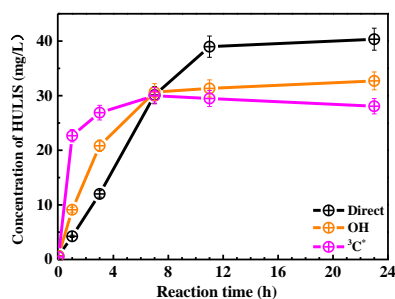
Figure 7. HULIS concentrations as a function of reaction time ~~for the three conditions~~under direct photolysis, OH-initiated oxidation and ³C*-initiated oxidation.

3.5 Mass yield and oxidation degree of reaction products

3.5.1 Mass yields

HULIS is only a subset of the products from aqueous oxidation, and here we used AMS to further quantify the total reaction products. Figure 8a shows SP-AMS measured organic mass profiles (normalized by sulfate mass, $\Delta Org/SO_4^{2-}$) against the reaction time. As the reaction propagated, $\Delta Org/SO_4^{2-}$ increased continuously in ³C*-initiated system. Nevertheless it arose stepwise and reached a maximum at 19 hours, then remained at a plateau for the direct photolysis and OH-mediated oxidation. Figure 8b illustrates the calculated mass yields at different reaction times. The mass yields ~~after 1 hour of illumination~~ were in the ranges of 46.2%-196.5%, 22.1%-144.9%, 19.3%-140.1% for ³C*-oxidation, OH-oxidation and direct photolysis, respectively. For the same oxidation time, mass yield from ³C*-oxidation was generally higher than those from OH-oxidation and direct photolysis. There are two plausible reasons for high mass yield of ³C*-initiated oxidation. First, oxidation by ³C* was more efficient to form oligomers and functionalized/oxygenated products (Richards-Henderson et al., 2014;

626 Yu et al., 2016). Higher oxidative degree of products from ^{3}C*-initiated photooxidation

627 (see Sec.3.5.2) supports this hypothesis. Secondly, more light-absorbing products

628 formed during initial stage of ^{3}C*-oxidation (Fig. 5c) may accelerate oxidation by

629 acting as photosensitizers (Tsui et al., 2018).

630 The product mass yields obtained in this work (~20%-197%) overall agree with

631 those reported previously for phenolic compounds. For examples, Huang et al. (2018)

632 reported mass yields of 30-120% for syringaldehyde and acetosyringone; Smith et al.

633 (2014) found that mass yields of aqSOA from three phenols with ^{3}C* were nearly 100%,

634 and Ma et al. (2021) reported a yield ranging from 59 to 99% for six highly substituted

635 phenols with ^{3}C*; Mass yields of SOA from three benzene-diols were near 100% with

636 both OH and ^{3}C* oxidants (Smith et al., 2015); Direct photolysis of phenolic carbonyls,

637 and oxidation of syringol by ^{3}C*, had SOA mass yields ranging from 80 to 140% (Smith

638 et al., 2016). Our previous study on eugenol OH oxidation illuminated by a 500 W Xe

639 lamp reported a mass yield of ~180% (Ye et al., 2020), slightly higher than the value

640 determined here owing to different ~~simulated lights~~light wavelengths/intensities.
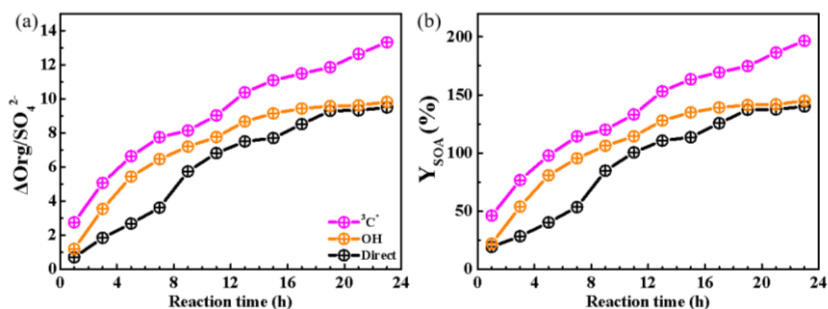
641

642 **Figure 8.** Variations of the organic mass normalized by sulfate (a) (ΔOrg/SO$_4$$^{2-}$) and (b) mass yields

643 of reaction products with reaction time under ~~three conditions~~direct photolysis, OH-initiated

644 oxidation and ^{3}C*-initiated oxidation.

645

646 **3.5.2 Oxidation degree**

647   In order to further probe oxidation levels of the reaction products, O/C derived

648   from SP-AMS mass spectrum of the organics was used to represent the oxidation degree

649   of products. In addition, carbon oxidation state (OSc, defined as 2*O/C - H/C) (Kroll

650   et al., 2011) was also calculated ~~(Kroll et al., 2011).~~. Figures 9a-c depict variations of

651   the elemental ratios (O/C and H/C) and OSc during oxidations. Dramatic increases of

652   O/C and OSc during the initial stage of oxidation (within 1 hour) were observed, with

653   O/C changing from 0.26 to 0.65, from 0.26 to 0.70, from 0.25 to 0.75, as well as OSc

654   from -1.11 to -0.15, from -1.16 to -0.05, from -1.13 to 0.09 for direct photolysis, OH-

655   oxidation and ^{3}C*-oxidation, respectively. The O/C was lower than those of other

656   phenolic aqSOA (Yu et al., 2014) due to different substituted groups in aromatic ring of

657   the precursors. Both O/C and OSc gradually increased, while H/C changed little after 1

658   hour. The enhancements of OSc in the end were 1.22, 1.11 and 0.86 for ^{3}C*-initiated

659   oxidation, OH-initiated oxidation and direct photolysis, respectively.

660   Furthermore, the f_{44} vs. f_{43} diagram ("triangle plot") can be used to demonstrate

661   the evolution of SOA during oxidation (Ng et al., 2010). The f_{44} and f_{43} are defined as

662   the ratios of signal intensities of m/z 44 (mainly CO_2^+) and 43 (mainly $C_2H_3O^+$) to the

663   total organics. The results that the f_{44} increased continuously (moved upwards) during

664   both OH and ^{3}C* oxidations, indicating persistent formation of highly oxygenated

665   compounds including organic acids, such as formic acid and oxalic acid (Sun et al.,

666   2010). ~~Concentrations of organic acids increased with photochemical reactions can~~

667   ~~support this assumption (data not shown).~~ Note the f_{44} enhancement was much more

668   significant for ^{3}C* oxidation (from 0.07 to 0.16) than direct photolysis (from 0.07 to

669   0.12) and OH oxidation (from 0.07 to 0.13), consistent with the behaviors of its higher

670   O/C and OSc. The f_{43} value decreased in the first stage (1-3 hours) and then increased

671   at later stages. The final f_{43} values were almost the same as those of the initial solutions~~.~~

672 and were small. As a result, all data points located outside the f_{44} vs. f_{43} spacef_{43} region

673 (bounded by the two dash lines in Figs. 9d-f) for ambient aerosols established by Ng et

674 al. (2010) for ambient aerosols, owing to the relatively low f_{43} values.).

In summary, our results shown here demonstrate that aqueous phase eugenol

676 photochemical oxidation can generate highly oxygenated products and hence increase

677 the degree of oxygenation of overall SOA.
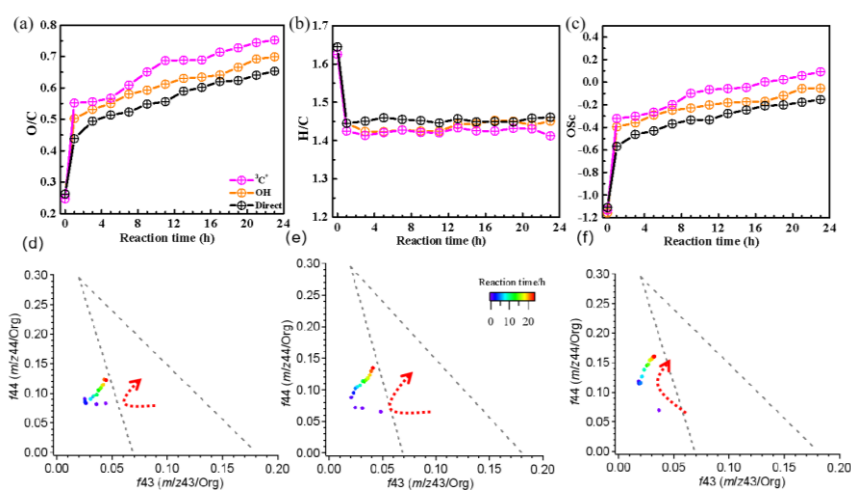
Figure 9. Variations of the elemental ratios of (a) O/C, (b) H/C and (c) the oxidation state (OSc) as

a function of reaction time, and the: f_{44} vs. f_{43} plots of reaction products under (ad) direct photolysis,

(be) OH-initiated oxidation, and (ef) $^{3}C^{*}$-initiated oxidation.

3.6 Molecular characterization of reaction products and proposed reaction mechanism

3.6.1 Major products identified by GC-MS

SP-AMS was limited to probe bulk composition of low-volatility oxidation

686 products, thus the molecular-level characterization of products was performed by using

687 GC-MS here. The total ion chromatograph (TIC) of GC-MS on the solutions before
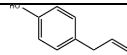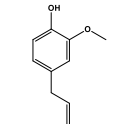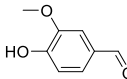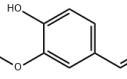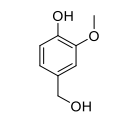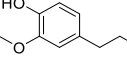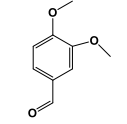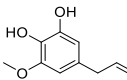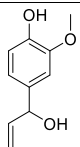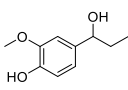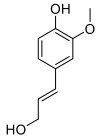
illumination (0 hour) and at illumination times of 11 and 23 hours for the $^3C^*$-initiated

photooxidation is shown in Fig. S7. As shown in Fig.S7, eugenol (retention time (RT)

at 11.50 min) loss was more than 90% at 11 hours, which could be confirmed by the

experimental data reported in Section 3.1. Comparison of products at 11 hours and 23

hours showed no significant difference. Similar to aqueous photochemical oxidation

with OH (Ye et al., 2020), a series of products were identified and listed in Table 2.

Except 5-ally-3-methoxybenzene-1,2-diol (MW 180, RT=12.59 min), the other eight

products were detected for both OH and $^3C^*$-initiated photooxidations. Some of them

(Eugenol, DMB, product 1, 2, 5) were identified by using certified reference materials,

some of them (product 3, 4, 6, 7, 8, 9) were inferred according to the molecular ion

peaks and fragments from GC-MS, based on spectra from the NIST database (Stein,

2014) and on the reactants and reaction conditions.

We also found 4-(1-hydroxypropyl)-2-methoxyphenol (product 8) was relatively

abundant (Fig.S7), suggesting functionalization might dominates as compared to

oligomerization and fragmentation. Products were mainly from addition/elimination of

hydroxyl (-OH), methoxyl (-OCH$_3$) to benzene ring or allyl group and further oxidized

to carbonyl or carboxyl compounds. As suggested by Bonin et al. (2007), the OH-

addition to the aromatic ring of phenol preferentially takes place at the ortho (48%) and

the para (36%) positions, leading to the formation of OH-adduct product 6 (5-allyl-3-

methoxybenzene-1,2-diol). Notably, dimers and ring-opening products were not

observed, but they cannot be excluded since they would be probably out of the detection

of GC-MS technique (Vione et al., 2014).

711   **Table 2.** Major reaction products identified via GC-MS

	RT (min)	Name*	Proposed chemical structure	Chemical formula	Nominal MW (g/mol)
Product 1	10.68	4-allylphenol		$C_9H_{10}O$	134
Precursor	11.50	Eugenol		$C_{10}H_{12}O_2$	164
Product 2	11.81	4-hydroxy-3-methoxybenzaldehyde		$C_8H_8O_3$	152
Product 3	12.06	(E)-2-methoxy-4-(prop-1-en-1-yl)phenol		$C_{10}H_{12}O_2$	164
Product 4	12.11	4-(hydroxymethyl)-2-methoxyphenol		$C_8H_{10}O_3$	154
Product 5	12.18	2-methoxy-4-propylphenol		$C_{10}H_{14}O_2$	166
Photosensitizer	12.29	3,4-dimethoxybenzaldehyde(DMB)		$C_9H_{10}O_3$	166
Product 6**	12.59	5-allyl-3-methoxybenzene-1,2-diol		$C_{10}H_{12}O_3$	180

Product 7	12.65	4-(1-hydroxyallyl)-2-methoxyphenol		$C_{10}H_{12}O_3$	180
Product 8	12.79	4-(1-hydroxypropyl)-2-methoxyphenol		$C_{10}H_{14}O_3$	182
Product 9	12.91	(E)-4-(3-hydroxyprop-1-en-1-yl)-2-methoxyphenol		$C_{10}H_{12}O_3$	180

*Precursor (eugenol) and triplet precursor (DMB) are also shown.

**This compound was only identified in $^3C^*$-oxidation solution.

3.6.2 Reaction mechanism

The reaction pathways of $^3C^*$-initiated photooxidation of eugenol are demonstrated in Scheme 1 based on the products identified by GC-MS. The other intermediates and the potential pathways were proposed according to the identified products and the reaction rationality from the starting reactant. To better depict the mechanism, DMB was expressed as [RCHO] and eugenol as Ph-R for simplicity. First, [RCHO] absorbs light and undergoes excitation to $^1[RCHO]^*$, then experiences the intersystem crossing (ISC) to form $^3[RCHO]^*$. $^3[RCHO]^*$ can participate in subsequent reactions via three channels. First, it can react with O_2 to form $^1O_2$ via energy transfer. Secondly, it can transform to $[RCHO]^{\cdot-}$, subsequently reacts with O_2 to generate $O_2^{\cdot-}$ via electron transfer, which can disproportionate to H_2O_2. The decomposition of H_2O_2 can generate OH radical. Thirdly, the $^3[RCHO]^*$ can react with Ph-R to from [Ph-R•] via H-abstraction. The cleavage of [Ph-R•] to free radical segment

727 (such as $CH_2CH\bullet$ or $CH_3O\bullet$) takes place, then an additional hydrogen transfer could

728 occur, resulting in a 2H-addition to the new intermediate to form 4-allyl-phenol

729 (product 1). Similarly, when the $CH_2CH\bullet$ is lost from [Ph-R$\bullet$], an addition of H_2O

730 would happen on the new compound (product 4) and further oxidized to 4-hydroxy-3-

731 methoxybenzaldehyde (product 2). Another possibility is the intermediate [Ph-R$\bullet$] can

732 resonate to several different isoelectronic species, the radical position changes to

733 aromatic ring or allyl group site, which would couple with HO$\bullet$ to form hydroxylated

734 eugenol monomer (product 6, 7, 9 MW=180). Consequently, the isoelectronic species

735 at allyl group site could also abstract a hydrogen to form isoeugenol (product 3

736 MW=164). Also, breakage of C=C into C-C and 2H-addition at allyl group site could

737 form 2-methoxy-4-propyl-phenol (product 5, MW=166). Besides, the C=C breaking

738 intermediate can couple with HO$\bullet$ to form 4-(1-hydroxypropyl)-2-methoxyphenol

739 (product 8, MW=182). In conclusion, $^3C^*$ can directly oxidize eugenol to form SOA

740 products or small molecular compounds, or indirectly oxidize eugenol via energy

741 transfer, electron transfer, hydrogen abstraction, proton-coupled electron transfer or

742 other radical chain reactions.

743   The organic groups, such as methoxy, allyl groups can be eliminated from

744 aromatic ring, which then participate in photochemical reaction, resulting in generation

745 of dimers, small organic acids, CO_2 and H_2O, etc. Dimers previously reported from

746 aqueous reaction of 4-methylsyringol with OH were not detected via GC-MS in the

747 present work but dimer fragment ions ($C_{20}H_{22}O_4^+$) were detected by SP-AMS with trace

748 amounts. Functionalization due to the additions of hydroxyl, carbonyl functional groups

749 to the aromatic rings could account for the enhancement of light absorption at

750 wavelength of 300-400 nm. However, polar high MW organic acids were not detected

751 likely due to the limitation of GC-MS technique.

752
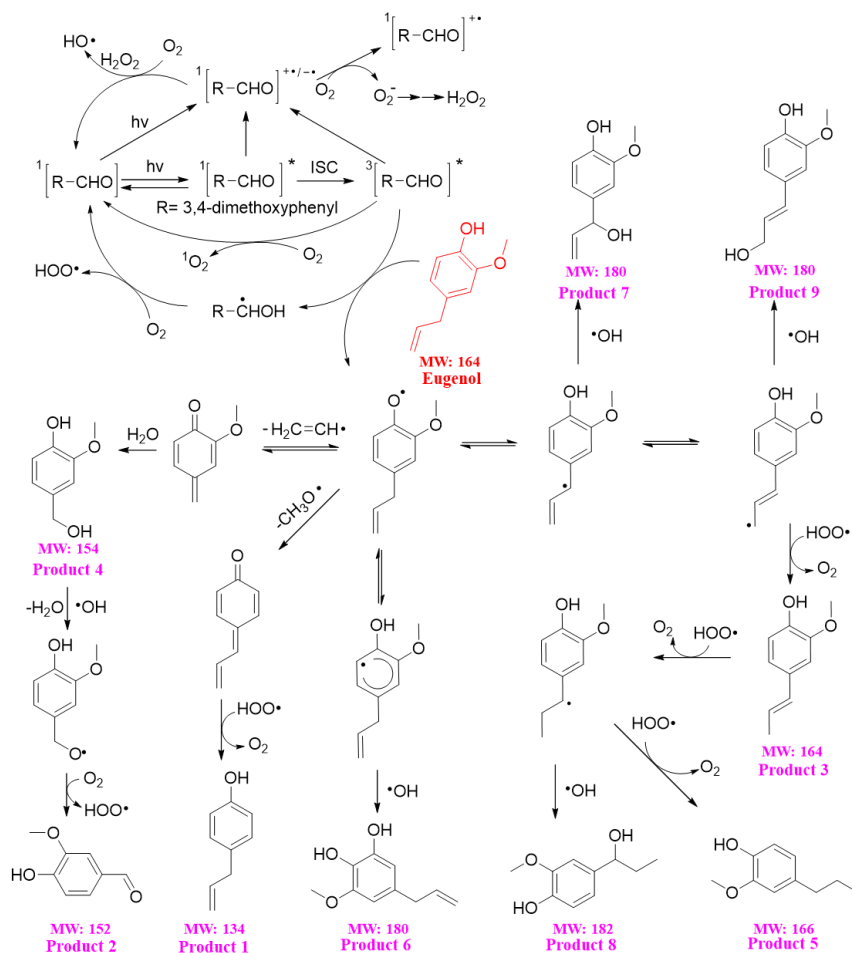
Scheme 1. Proposed reaction mechanism of $^{3}C^{*}$-initiated photooxidation of eugenol. The red ~~texts~~ ~~represent~~text represents the ~~products listed in Table 2~~precursor, and the compounds labeled by Product 1-9 are those identified by GC-MS~~.~~ (Table 2).

3.7 Oxidative potential (OP) of reaction products

~~Previous laboratory studies (Verma et al., 2015b; Xu et al., 2020) have confirmed that HULIS is a major constituent contributing to ROS-generation potential. As HULIS is an important fraction of the products from aqueous photooxidation of eugenol in this~~

760 ~~work (Fig. 7), here we investigated the links between the OPs and reaction products.~~

761 The OP of oxidation products can be represented by the consumption rate of DTT

762 concentration ~~per minute~~, defined as R_{DTT}. Figure 10a shows the DTT consumed mass

763 (M_{DTT}) as a function of incubation times (0, 30, 60, 90, 120 and 150 min) for a triplicate

764 sample (300 μM eugenol) and blank (ultrapure water). M_{DTT} values for both blank and

765 eugenol were proportional to incubation time, indicating that ROS-generating

766 substances in reaction solution act only as catalyst and itself was not consumed. The

767 slopes represent DTT consumption rates, which are also illustrated in Fig. 10a. Average

768 R_{DTT0} (blank) was 0.31 μM/min and R_{DTT} for initial 300 μM eugenol (before experiment)

769 was 0.52 μM/min. Since self-oxidation of DTT might lead to the consumption of DTT

770 in ultrapure water, final DTT consumption rate of reacted solution after

771 ~~photolysis~~oxidation was then blank-corrected by subtracting the average R_{DTT0}.

772 Figure 10b shows changes of blank-corrected R_{DTT} with ~~photolysis~~reaction time

773 for direct photolysis, OH-initiated oxidation and $^3C^*$-initiated oxidation, respectively.

774 The R_{DTT} value of $^3C^*$-oxidation products increased quickly and reached the maximum

775 (0.9) at 7 hours, then decreased slowly and its end value was lower than that from OH-

776 oxidation. The R_{DTT} value of OH-oxidation products on the other hand increased slowly

777 and reached the maximum at 21 hours. The R_{DTT} value of products from direct

778 photolysis increased continuously but also slowly to ~0.36 till the end of oxidation.

779 Nevertheless, we can see that the final R_{DTT} values were all higher than that of ~~initial~~

780 eugenol, proving that aqueous-phase processing can generate products with higher OP,

781 resulting in more health hazards than the precursor does. The DTT consumption rates

782 are comparable to those using the same DTT method (Charrier and Anastasio, 2012;

783 Lin and Yu, 2019). ~~This finding further indicates the effectiveness of DTT method to~~

784 ~~represent OP.~~The weak correlation was found between HULIS concentration and R_{DTT},

implying that OP was not only dependent upon HULIS. Moreover, HULIS with diverse

molecular structures also exhibit different ROS-generation potentials (Kramer et al.,

2016), therefore the HULIS as an ensemble may not correlate well with OP.
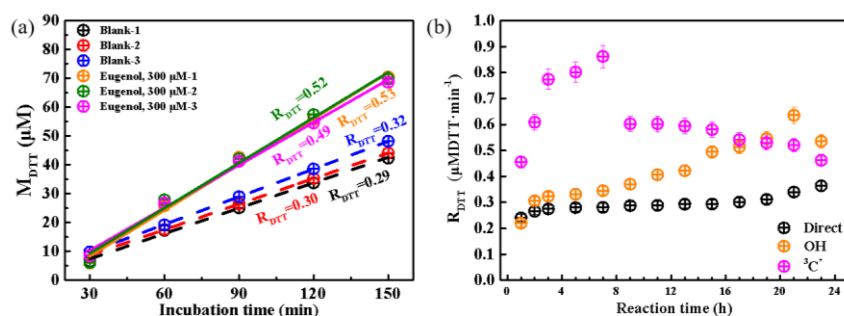
Figure 10. (a) DTT consumed mass versus incubation times for blank (ultrapure water) and 300 μM

eugenol solutions in a triplicate, and (b) blank-corrected DTT consumption rates versus reaction

time for direct photolysis, OH-initiated oxidation and $^3C^*$-induced oxidation.

4. Atmospheric implications

The high mass yields of aqueous-phase photooxidation of eugenol (exceeding 100%

after 23 hours of illumination) ~~studied~~found here are similar or even higher than those

previously reported yields of a number of phenolic compounds (e.g., Smith et al., 2014,

2015, 2016; Ma et al., 2021), which re-emphasizes the importance of biomass burning

(BB) to SOA budget (Gilardoni et al., 2016), particularly in regions or periods with

significant BB activities. ~~Compared to simple phenols (such as syringol) that are only~~

~~present in cloud/fog waters, the highly substituted phenols are able to significantly~~

~~partition into aerosol water too (Ma et al., 2021). Since the highly substituted phenols~~

~~can take up roughly 30–45% of total phenols emitted from wood burning (Schauer et~~

~~al., 2001), our results further imply that aqueous production of SOA from BB emissions~~

~~can not only occur in fog/cloud conditions, but also in common humid weather~~

804 conditions, highlighting the general importance of aqueous oxidation pathway to SOA.

805 ~~Our~~In addition, our study here used 300 μM H_2O_2 and 15 μM DMB as sources of

806 OH and $^3C^*$, and $^3C^*$-mediated oxidation appeared to be faster than OH-initiated

807 oxidation of eugenol. Of course, whether or not $^3C^*$ is more important than OH in real

808 atmosphere depends upon their concentrations. OH and $^3C^*$ are difficult to measure and

809 concentrations vary greatly in real atmospheric samples. Herrmann et al. (2010)

810 estimated an average OH level of 0.35×10^{-14} M in urban fog water; Kaur and Anastasio

811 (2018) measured $^3C^*$ concentration to be $(0.70\text{-}15) \times 10^{-14}$ M, 10-100 times higher than

812 the co-existing OH in ambient fog waters; Kaur et al. (2019) determined both OH and

813 $^3C^*$ concentrations in PM extracts, OH steady-state concentration was $4.4(\pm2.3) \times 10^{-16}$

814 M, similar to its level in fog, cloud and rain, while $^3C^*$ concentration was $1.0(\pm0.4)$

815 $\times 10^{-13}$ M, a few hundred times higher than OH and nearly double its average value in

816 fog. Therefore, together with these measurements, our findings signify a likely more

817 important role of $^3C^*$ than OH in aqueous-phase (especially aerosol water) reactions.

818 ~~In addition~~However, the liquid water content of aerosol is typically ~10000 times

819 smaller than that of cloud (for instance, ~50 μg m^{-3} versus 0.5 g m^{-3}). Even if the

820 reaction rates in aerosol water were 10 times higher than those in cloud water, the

821 overall importance of aqueous reactions initiated by the same oxidant in aerosol phase

822 would be still ~1000 times smaller than it in cloud water. Moreover, quenching

823 experiments reveal that O_2 can inhibit eugenol degradation by effectively scavenging

824 $^3C^*$ ~~radical~~ while it can promote degradation by fostering ~~radical~~ chain reactions in OH-

825 induced oxidation, which offer insights to the control of reaction pathways by

826 regulating ~~the~~ ROS generations; of course, such operation calls for application of highly

827 sensitive EPR method.

828 Eugenol has a strong light absorption peak around 280 nm, therefore it can

photolyze itself undergo direct photolysis, and addition of OH or other photosensitizers (³C*) can gradually diminish its light absorption around 280 nm, but increase the absorption in visible light range (>300 nm). In the meantime, HULIS was generated continuously, and GC-MS identified a number of high MW organic products, in line with those detected in earlier aqueous photooxidation of phenolic compounds (Jiang et al., 2021; Misovich et al., 2021; Tang et al., 2020; Yu et al., 2014). Overall, our work demonstrates that aqueous oxidation of BB emissions is a source of BrC, and this BrC may act as photosensitizer to oxidize other species; a portion of this BrC might be HULIS, and some high MW aromatic compounds are a subset of this HULIS. However, a recent study by Wang et al. (2021) shows that fossil foil derived OA (FFOA) can be an effective precursor of aqSOA, but the aqSOA became less light-absorbing than the FFOA. Aqueous oxidation of 4-nitrophenol with OH can lead to a photobleaching effect too (Witkowski et al., 2022). These contrasting results indicate that contribution of aqueous oxidation to BrC is largely dependent upon the precursors; molecular structures of major chromophores, changes of the structures upon oxidation as well as their interplay with light absorptivity should be carefully investigated to achieve a full understanding of the impacts of aqueous processing on air quality, radiative forcing and climate change.

Investigations on the OPs of reaction products from eugenol photooxidation in all three conditions show that aqueous processing can produce more toxic products than its the precursor. This result is in agreement with our previous work on resorcinol, hydroquinone and methoxyhydroquinone (Ou et al., 2021). Although more studies on a broad spectrum of atmospherically relevant species and multiple indicators of toxicity are clearly needed, our findings here underscore the potential of aqueous processing on the enhancement of particle toxicity. Considering high PM concentration is often

5 Conclusions

This study comprehensively investigated the aqueous photooxidation of eugenol upon direct photolysis and attacks by OH radicals and $^3C^*$ radicals triplet states. By using a suite of techniques, the decay kinetics of eugenol, chemical, optical properties as well as toxicity of reaction products were systematically studied. The first-order photolysis rate constants followed the order of $^3C^*$>OH >direct photolysis (300 μM H_2O_2 and 15 μM DMB as sources of OH and $^3C^*$). Further quenching experiments on different ROS during $^3C^*$-mediated oxidation showed that $^3C^*$ was the major contributor, followed by $^1O_2$, $O_2^{\bullet-}$ and OH; $O_2^{\bullet-}$ played a more important role than OH during OH-initiated oxidation. Photolysis The rate constants under saturated O_2, air and N_2 followed the order of $k_{O_2} > k_{Air} > k_{N_2}$ for both direct photolysis and OH-initiated oxidation, but changed to $k_{Air} > k_{N_2} > k_{O_2}$ for $^3C^*$-mediated oxidation. O_2 appeared to be a scavenger of $^3C^*$ therefore suppressing $^3C^*$ oxidation while it could promote generation of OH thus accelerate OH-mediated oxidation. pH and DO levels both decreased during oxidation, indicating formation of acids and a certain role of DO in oxidation.

Eugenol itself can absorbs lights significantly around 280 nm, and aqueous oxidation gradually decrease this absorption of UV light but enhanced the absorbance in the visible light range (mainly 300-400 nm), indicative of the generation of BrC species. These species were likely linked with HULIS, as HULIS concentration increased during the course of oxidation, in particular for the initial stage of $^3C^*$-mediated reactions. The final mass yields of reaction products (after 23 hours of

878 irradiation) were 140.1%, 144.9% and 196.5% for direct photolysis, OH-oxidation and

879 $^3C^*$-oxidation, respectively. Oxidation degrees of the products increased continuously

880 with the illumination time, indicating persistent formation of highly oxygenated

881 compounds, especially during $^3C^*$-mediated reactions. Molecular characterization by

882 GC-MS identified a series of oxygenated compounds, allowing us to propose the

883 detailed oxidation mechanism. Functionalization appeared to be a dominant pathway to

884 form the observed species.

885   DTT method was used to assess ~~OPs~~OP of the reaction products. The end products

886 in all three ~~cases~~sets of experiments showed higher DDT consumption rates than that

887 of the precursor; products from $^3C^*$-oxidation showed particularly fast increase in the

888 first few hours of reactions. This result demonstrates that species that are more toxic

889 than its precursors could be produced upon aqueous oxidation, indicative of the

890 potential toxic effects induced by aqueous processing. ~~Overall, by using eugenol as a~~

891 ~~model compound of BB emissions, our findings highlight the importance of aqueous~~

892 ~~oxidation of BB emissions to SOA formation, its potentially important role in affecting~~

893 ~~radiative balance and climate through formation of BrC, as well as possible additional~~

894 ~~adverse health effects. Such effects should be considered in air quality or climate~~

895 ~~models to better assess the influence of BB emissions.~~

896

897 ***Data availability.*** The relevant data ~~in~~of this study are available ~~from the authors upon~~

898 ~~request   (bess_ye@jsut.edu.cn   or   caxinra@163.com)~~at:

899 http://nuistairquality.com/eugenol_data_and_figure

900

901 ***Supplement.*** The supplement related to this article is available on line at: XXX

902

903 *Author Contributions:* XDL, YT, LWZ, SSM, SPL, ZZZ and NS conducted the

904 experiments. XDL and YT analyzed the data. XDL and ZLY prepared and wrote the

905 paper with contributions from all co-authors. ZLY and XLG reviewed and commented

906 on the paper.

907

908 *Competing interests.* The authors declare that they have no conflict of interest.

909

910 *Acknowledgements.* The authors acknowledge support from the National Natural

911 Science Foundation of China (21976093 and 42021004), the Natural Science

912 Foundation of Jiangsu Province (BK20181476), open fund by Jiangsu Key Laboratory

913 of Atmospheric Environment Monitoring and Pollution Control (KHK1904) and the

914 Postgraduate Research & Practice Innovation Program of Jiangsu Province

915 (SJCX21_1332, SJCX20_1030) and of Jiangsu University of Technology

916 (XSJCX20_05).

917

918 *Financial support:* This research was funded by the National Natural Science

919 Foundation of China (21976093 and 42021004), the Natural Science Foundation of

920 Jiangsu Province (BK20181476), and open fund by Jiangsu Key Laboratory of

921 Atmospheric Environment Monitoring and Pollution Control (KHK1904).

922

923 *Review statement.* This paper was xxx

924 # References

925 Alam, M. S., Delgado-Saborit, J. M., Stark, C., and Harrison, R. M.: Using atmospheric measurements

926   of PAH and quinone compounds at roadside and urban background sites to assess sources and

927   reactivity, Atmos. Environ., 77(3), 24-35, https://doi.org/10.1016/j.atmosenv.2013.04.068, 2013.

928   Alegría, A. E., Ferrer, A., Santiago, G., Sepúlveda, E., and Flores, W.: Photochemistry of water-soluble

929   quinones. Production of the hydroxyl radical, singlet oxygen and the superoxide ion, J.

930   Photochem. Photobiol. Chem., 127, 57-65, https://doi.org/10.1016/S1010-6030(99)00138-0,

931   1999.

932   Arakaki, T., Anastasio, C., Kuroki, Y., Nakajima, H., Okada, K., Kotani, Y., Handa, D., Azechi, S.,

933   Kimura, T., Tsuhako, A., and Miyagi, Y.: A general scavenging rate constant for reaction of

934   hydroxyl radical with organic carbon in atmospheric waters, Environ. Sci. Technol., 47, 8196-

935   8203, https://doi.org/10.1021/es401927b, 2013.

936   Aryal, R., Lee, B. K., Beecham, S., Kandasamy, J., Aryal, N., and Parajuli, K.: Characterisation of road

937   dust organic matter as a function of particle size: A PARAFAC Approach, Water Air Soil Poll.;

938   226, https://doi.org/10.1007/s11270-014-2289-y, 2015.

939   Bari, M, A, Baumbach, G., Kuch, B., and Scheffknecht, G.. Wood smoke as a source of particle-

940   phase organic compoundsin residential areas, Atmos. Environ., 43, 4722-4732,

941   https://doi.org/10.1016/j.atmosenv.2008.09.006, 2009.

942   Barzaghi, P. and Herrmann, H.: A mechanistic study of the oxidation of phenol by $OH/NO2/NO_3$ in

943   aqueous solution, Phys. Chem. Chem. Phys., 4, 3669-3675,

944   https://doi.org/10.1039/B201652D, 2002.

945   Barsotti, F., Ghigo, G., and Vione, D. Computational assessment of the fluorescence emission of

946   phenol oligomers: A possible insight into the fluorescence properties of humic-like Substances

947   (HULIS), J. Photochem. Photobio. A, 315, 87-93,

948   https://doi.org/10.1016/j.jphotochem.2015.09.012, 2016.

949   Bianco, A., Minella, M., De Laurentiis, E., Maurino, V., Minero, C., and Vione, D. Photochemical

950   generation of photoactive compounds with fulvic-like and humic-like fluorescence in aqueous

951   solution, Chemosphere, 111, 529-536, https://dx.doi.org/10.1016/j.chemosphere.2014.04.035,

952   2014.

953   Bonin, J., Janik, I., Janik, D. and Bartels, D. M.: Reaction of the hydroxyl radical with phenol in water

954   up to supercritical conditions, J. Phys. Chem. A, 111(10), 1869-1878,

955   https://doi.org/10.1021/jp0665325, 2007.

956   Canagaratna, M. R., Jimenez, J. L., Kroll, J. H., Chen, Q., Kessler, S. H., Massoli, P., Hildebrandt Ruiz,

957   L., Fortner, E., Williams, L. R., Wilson, K. R., Surratt, J. D., Donahue, N. M., Jayne, J. T., and

958   Worsnop, D. R.: Elemental ratio measurements of organic compounds using aerosol mass

959   spectrometry: characterization, improved calibration, and implications, Atmos. Chem. Phys.,

960   15, 253-272, https://doi.org/10.5194/acp-15-253-2015, 2015.

961   Chang, J. L., and Thompson, J. E.: Characterization of colored products formed during irradiation of

962   aqueous solutions containing H_2O_2 and phenolic compounds, Atmos. Environ., 44, 541-551,

963   https://doi.org/10.1016/j.atmosenv.2009.10.042, 2010.

964   Charrier, J. G., and Anastasio, C.: On dithiothreitol (DTT) as a measure of oxidative potential for ambient

965   particles: evidence for the importance of soluble transition metals, Atmos. Chem. Phys. 12,

966   9321-9333, https://doi.org/10.5194/acp-12-9321-2012, 2012.

967   Chen, H., Ge, X., Ye, Z.: Aqueous-phase secondary organic aerosol formation via reactions with organic

968   triplet   excited   states—a   short   review.   Curr.   Pollut.   Rep.,   4,   8-12,

969   https://doi.org/10.1007/s40726-018-0079-7, 2018.

970   Chen, Q., Ikemori, F., and Mochida, M.: Light Absorption and excitation-emission fluorescence of urban

971   organic aerosol components and their relationship to chemical structure, Environ. Sci. Technol.,

972   50, 10859-10868, https://doi.org/10.1021/acs.est.6b02541, 2016a.

973   Chen, Q., Miyazaki, Y., Kawamura, K., Matsumoto, K., Coburn, S., Volkamer, R., Iwamoto, Y., Kagami,

974   S., Deng, Y., Ogawa, S., Ramasamy, S., Kato, S., Ida, A., Kajii, Y., and Mochida, M.:

975   Characterization of chromophoric water-soluble organic matter in urban, forest, and marine

976   aerosols by HR-ToF-AMS analysis and excitation-emission matrix spectroscopy, Environ. Sci.

977   Technol., 50, 10351-10360, https://doi.org/10.1021/acs.est.6b01643, 2016b.

978   Chen, Q., Wang, M., Wang, Y., Zhang, L., Li, Y., and Han, Y.: Oxidative potential of water-soluble matter

979   associated with chromophoric substances in $PM_{2.5}$ over Xi'an, China, Environ. Sci. Technol., 53,

980   8574-8584, https://doi.org/10.1021/acs.est.9b01976, 2019.

981   Chen, Y., Li, N., Li, X., Tao, Y., Luo, S., Zhao, Z., Ma, S., Huang, H., Chen, Y., Ye, Z., and Ge, X.:

982   Secondary organic aerosol formation from $^3C^*$-initiated oxidation of 4-ethylguaiacol in

983   atmospheric   aqueous-phase,   Sci.   Total.   Environ.,   723,   137953,

984   https://doi.org/10.1016/j.scitotenv.2020.137953, 2020.

985   Cho, A. K., Sioutas, C., Miguel, A. H., Kumagai, Y., Schmitz, D. A., Singh, M., Eiguren-Fernandez, A.,

986   and Froines, J. R.: Redox activity of airborne particulate matter at different sites in the Los

Angeles Basin, Environ. Res., 99, 40-7, https://doi.org/10.1016/j.envres.2005.01.003, 2005.

De Laurentiis, E., Sur, B., Pazzi, M., Maurino, V., Minero, C., Mailhot, G., Brigante, M., and Vione, D.: Phenol transformation and dimerisation, photosensitised by the triplet state of 1-nitronaphthalene: A possible pathway to humic-like substances (HULIS) in atmospheric waters, Atmos. Environ., 70, 318-327, https://doi.org/10.1016/j.atmosenv.2013.01.014, 2013.

Dou, J., Lin, P., Kuang, B. Y., and Yu, J.: Reactive oxygen species production mediated by humic-like substances in atmospheric aerosols: enhancement effects by pyridine, imidazole, and their derivatives, Environ. Sci. Technol., 49(11), 6457-6465, https://doi.org/10.1021/es5059378, 2015.

Ervens, B., Turpin, B. J., and Weber, R. J.: Secondary organic aerosol formation in cloud droplets and aqueous particles (aqSOA): a review of laboratory, field and model studies, Atmos. Chem. Phys., 11, 11069-11102, https://doi.org/10.5194/acp-11-11069-2011, 2011.

Fang, T., Verma, V., Bates, J. T., Abrams, J., Klein, M., Strickland, M. J., Sarnat, S. E., Chang, H. H., Mulholland, J. A., Tolbert, P. E., Russell, A. G., and Weber, R. J.: Oxidative potential of ambient water-soluble $PM_{2.5}$ in the southeastern United States: contrasts in sources and health associations between ascorbic acid (AA) and dithiothreitol (DTT) assays, Atmos. Chem. Phys., 16, 3865-3879, https://doi.org/10.5194/acp-16-3865-2016, 2016.

Faust, J. A., Wong, J. P., Lee, A. K., and Abbatt, J. P.: Role of aerosol liquid water in secondary organic aerosol formation from volatile organic compounds, Environ. Sci. Technol., 51, 1405-1413, https://doi.org/10.1021/acs.est.6b04700, 2017.

Ge, X., Li, L., Chen, Y., Chen, H., Wu, D., Wang, J., Xie, X., Ge, S., Ye, Z., Xu, J., and Chen, M. Aerosol characteristics and sources in Yangzhou, China resolved by offline aerosol mass spectrometry and other techniques. Environ. Pollut., 225, 74-85, https://doi.org/10.1016/j.envpol.2017.03.044, 2017.

George, K. M., Ruthenburg, T. C., Smith, J., Yu, L., Zhang, Q., Anastasio, C., and Dillner, A. M.: FT-IR quantification of the carbonyl functional group in aqueous-phase secondary organic aerosol from phenols, Atmos. Environ., 100, 230-237, https://doi.org/10.1016/j.atmosenv.2014.11.011, 2015.

Gilardoni, S., Massoli, P., Paglione, M., Giulianelli, L., Carbone, C., Rinaldi, M., Decesari, S., Sandrini, S., Costabile, F., Gobbi, G. P., Pietrogrande, M. C., Visentin, M., Scotto, F., Fuzzi, S., and Facchini, M. C.: Direct observation of aqueous secondary organic aerosol from biomass-

1017   burning emissions, Proc. Natl. Acad. Sci. USA., 113, 10013-10018,
1018   https://doi.org/10.1073/pnas.1602212113, 2016.

1019 Gligorovski, S., Strekowski, R., Barbati, S., and Vinoe, D.: Environmental implications of hydroxyl
1020   radicals (OH), Chem. Rev., 115(24), 13051-13092, https://doi.org/10.1021/cr500310b, 2015.

1021 Graber, E. R., and Rudich, Y.: Atmospheric HULIS: how humic-like are they? A comprehensive and
1022   critical review, Atmos. Chem. Phys., 6, 729-753, https://doi.org/10.5194/acp-6-729-2006,
1023   2006.

1024 Guo, Y., Zhang, Y., Yu, G., and Wang, Y., Revisiting the role of reactive oxygen species for pollutant
1025   abatement during catalytic ozonation: the probe approach versus the scavenger approach, Appl.
1026   Catal. B Environ., 280, 119418, https://doi.org/10.1016/j.apcatb.2020.119418, 2021.

1027 Hawthorne, S.B., Krieger M.S., Miller D.J., and Mathiason M.B. Collection and quantitation of
1028   methoxylated phenol tracers for atmospheric pollution from residential wood stoves, Environ. Sci.
1029   Technol., 23,470-475, https://doi.org/10.1021/es00181a013, 1989.

1030 He, L., Schaefer, T., Otto, T., Kroflic, A., and Herrmann, H.: Kinetic and theoretical study of the
1031   atmospheric aqueous-phase reactions of OH radicals with methoxyphenolic compounds, J. Phys.
1032   Chem. A, 123, 7828-7838, https://doi.org/10.1021/acs.jpca.9b05696, 2019.

1033 Herrmann, H.: Kinetics of aqueous phase reaction relevant for atmospheric chemistry, Chem. Rev., 103,
1034   4691-4716, https://doi.org/10.1021/cr020658q, 2003.

1035 Herrmann, H., Hoffmann, D., Schaefer, T., Bräuer, P. and Tilgner, A.: Tropospheric aqueous-phase free-
1036   radical chemistry: Radical sources, spectra, reaction kinetics and prediction tools.
1037   ChemPhysChem, 11, 3796-3822, https://doi.org/10.1002/cphc.201000533, 2010.

1038 Herrmann, H., Schaefer, T., Tilgner, A., Styler, S. A., Weller, C., Teich, M. and Otto, T.: Tropospheric
1039   aqueous-phase chemistry: kinetics, mechanisms, and its coupling to a changing gas phase,
1040   Chem. Rev., 115(10), 4259-4334, https://doi.org/10.1021/cr500447k, 2015.

1041 Hong, J., Han, B., Yuan, N., and Gu, J.: The roles of active species in photo-decomposition of organic
1042   compounds by microwave powered electrodeless discharge lamps, J. Environ. Sci. (China), 33,
1043   60-68, https://doi.org/10.1016/j.jes.2014.12.016, 2015.

1044 Huang, D., Zhang, X., Chen, Z. M., Zhao, Y., and Shen, X. L.: The kinetics and mechanism of an aqueous
1045   phase isoprene reaction with hydroxyl radical, Atmos. Chem. Phys., 11, 7399-7415,
1046   https://doi.org/10.5194/acp-11-7399-2011, 2011.

1047 Huang, D., Zhang, Q., Cheung, H. H. Y., Yu, L., Zhou, S., Anastasio, C., Smith, J. D., and Chan, C. K.:
1048   Formation and evolution of aqSOA from aqueous-phase reactions of phenolic carbonyls:
1049   comparison between ammonium sulfate and ammonium nitrate solutions, Environ. Sci.
1050   Technol., 52, 9215-9224, https://doi.org/10.1021/acs.est.8b03441, 2018.

1051 Huo, Y., Guo, Z., Li, Q., Wu, D., Ding, X., Liu, A., Huang, D., Qiu, G., Wu, M., Zhao, Z., Sun, H., Song,
1052   W., Li, X., Chen, Y., Wu, T., and Chen, J. Chemical fingerprinting of HULIS in particulate
1053   matters emitted from residential coal and biomass combustion, Environ. Sci. Technol., 55, 3593-
1054   3603. https://doi.org/10.1021/acs. est.0c08518, 2021.

1055 Jiang, W., Misovich, M. V., Hettiyadura, A. P. S., Laskin, A., McFall, A. S., Anastasio, C., and Zhang, Q.:
1056   Photosensitized reactions of a phenolic carbonyl from wood combustion in the aqueous phase-
1057   chemical evolution and light absorption properties of aqSOA, Environ. Sci. Technol., 55, 5199-
1058   5211, https://doi.org/10.1021/acs.est.0c07581, 2021.

1059 Kaur, R., and Anastasio, C.: First measurements of organic triplet excited states in atmospheric waters,
1060   Environ. Sci. Technol., 52, 5218-5226, https://doi.org/10.1021/acs.est.7b06699, 2018.

1061 Kaur, R., Labins, J. R., Helbock, S. S., Jiang, W., Bein, K. J., Zhang, Q., and Anastasio, C.: Photooxidants
1062   from brown carbon and other chromophores in illuminated particle extracts, Atmos. Chem.
1063   Phys., 19, 6579-6594, https://doi.org/10.5194/acp-19-6579-2019, 2019.

1064 Kramer, A.J., Rattanavaraha, W., Zhang, Z., Gold, A., Surratt, J.D., and Lin, Y.-H. Assessing the oxidative
1065   potential of isoprene-derived epoxides and secondary organic aerosol, Atmos. Environ., 130,
1066   211-218, https://dx.doi.org/10.1016/j.atmosenv.2015.10.018, 2016.

1067 Kroll, J. H., Donahue, N. M., Jimenez, J. L., Kessler, S. H., Canagaratna, M. R., Wilson, K. R., Altieri,
1068   K. E., Mazzoleni, L. R., Wozniak, A. S., Bluhm, H., Mysak, E. R., Smith, J. D., Kolb, C. E., and
1069   Worsnop, D. R.: Carbon oxidation state as a metric for describing the chemistry of atmospheric
1070   organic aerosol, Nat. Chem., 3, 133-9, https://doi.org/10.1038/nchem.948, 2011.

1071 Laurentiis, E. D., Socorro, J., Vione, D., Quivet, E., Brigante, M., Mailhot, G., Wortham, H., and
1072   Gligorovski, S.: Phototransformation of 4-phenoxyphenol sensitised by 4-
1073   carboxybenzophenone: evidence of new photochemical pathways in the bulk aqueous phase and
1074   on the surface of aerosol deliquescent particles, Atmos. Environ., 8, 569-578,
1075   https://doi.org/10.1016/j.atmosenv.2013.09.036, 2013.

1076 Lee, A. K. Y., Hayden, K. L., Herckes, P., Leaitch, W. R., Liggio, J., Macdonald, A. M., and Abbatt, J. P.

1077   D.: Characterization of aerosol and cloud water at a mountain site during WACS 2010: secondary

1078   organic aerosol formation through oxidative cloud processing, Atmos. Chem. Phys., 12, 7103-7116,

1079   https://doi.org/10.5194/acp-12-7103-2012, 2012.

1080   Leenheer, J. A., and Croue, J. P. Characterizing aquatic dissolved organic matter, Environ. Sci.

1081   Technol., 37, 18A-26A, https://doi.org/10.1021/es032333c, 2003.

1082   Li, F., Tsona, N. T., Li, J., and Du, L.: Aqueous-phase oxidation of syringic acid emitted from biomass

1083   burning: formation of light-absorbing compounds, Sci. Total Environ., 765, 144239,

1084   https://doi.org/10.1016/j.scitotenv.2020.144239, 2021.

1085   Li, Y. J., Huang, D. D., Cheung, H. Y., Lee, A. K. Y., and Chan, C. K.: Aqueous-phase photochemical

1086   oxidation and direct photolysis of vanillin-a model compound of methoxy phenols from biomass

1087   burning, Atmos. Chem. Phys., 14, 2871-2885, https://doi.org/10.5194/acp-14-2871-2014, 2014.

1088   Lim, Y. B., Tan, Y., Perri, M. J., Seitzinger, S. P., and Turpin, B. J.: Aqueous chemistry and its role in

1089   secondary organic aerosol (SOA) formation, Atmos. Chem. Phys., 10, 10521-10539,

1090   https://doi.org/10.5194/acpd-10-14161-2010, 2010.

1091   Lin, M., and Yu, J. Z.: Dithiothreitol (DTT) concentration effect and its implications on the applicability

1092   of DTT assay to evaluate the oxidative potential of atmospheric aerosol samples, Environ.

1093   Pollut., 251, 938-944, https://doi.org/10.1016/j.envpol.2019.05.074, 2019.

1094   Ma, L., Guzman, C., Niedek, C., Tran, T., Zhang, Q. and Anastasio, C.: Kinetics and mass yields of

1095   aqueous secondary organic aerosol from highly substituted phenols reacting with a triplet excited

1096   state, Environ. Sci. Technol., 55(9), 5772-5781, doi:10.1021/acs.est.1c00575, 2021.

1097   Ma, Y., Cheng, Y., Qiu, X., Cao, G., Kuang, B., Yu, J.Z., and Hu, D. Optical properties, source

1098   apportionment and redox activity of Humic-Like Substances (HULIS) in airborne fine

1099   particulates in Hong Kong, Environ. Pollut., 255,113087,

1100   https://doi.org/10.1016/j.envpol.2019.113087, 2019.

1101   Mabato, B. R. G., Lyu, Y., Ji, Y., Li, Y., Huang, D., Li, X., Nah, T., Lam, C. H., and Chan, C. K.: Aqueous

1102   secondary organic aerosol formation from the direct photosensitized oxidation of vanillin in the

1103   absence and presence of ammonium nitrate, Atmos. Chem. Phys., 22, 273-293,

1104   https://doi.org/10.5194/acp-22-273-2022, 2022.

1105   McWhinney, R. D., Zhou, S., and Abbatt, J. P. D.: Naphthalene SOA: redox activity and naphthoquinone

1106   gas–particle partitioning, Atmos. Chem. Phys., 13, 9731-9744, https://doi.org/10.5194/acp-13-

9731-2013, 2013.

Misovich, M. V., Hettiyadura, A. P. S., Jiang, W. Q., and Zhang, Q. Molecular-level study of the photo-oxidation of aqueous-phase guaiacyl acetone in the presence of ^{3}C*: formation of brown carbon products, ACS Earth Space Chem., 5, 1983-1996, https://doi.org/10.1021/acsearthspacechem.1c00103, 2021.

Mladenov, N, Alados-Arboledas, L., Olmo, F .J., Lyamani, H., Delgado, A., Molina, A., and Reche, I.: Applications of optical spectroscopy and stable isotope analyses to organic aerosol source discrimination in an urban area, Atmos. Environ., 45, 1960-1969, https://doi.org/10.1016/j.atmosenv.2011.01.029, 2011.

Nau, W. M., and Scaiano, J. C.: Oxygen quenching of excited aliphatic ketones and diketones, J. Phys. Chem., 100, 11360-11367, https://doi.org/10.1021/jp960932i, 1996.

Ng, N. L., Canagaratna, M. R., Zhang, Q., Jimenez, J. L., Tian, J., Ulbrich, I. M., Kroll, J. H., Docherty, K. S., Chhabra, P. S., Bahreini, R., Murphy, S. M., Seinfeld, J. H., Hildebrandt, L., Donahue, N. M., DeCarlo, P. F., Lanz, V. A., Prevot, A. S. H., Dinar, E., Rudich, Y., and Worsnop, D. R.: Organic aerosol components observed in Northern Hemispheric datasets from aerosol mass spectrometry, Atmos. Chem. Phys., 10, 4625-4641, https://doi.org/10.5194/acp-10-4625-2010, 2010.

Onasch, T. B., Trimborn, A., Fortner, E. C., Jayne, J. T., Kok, G. L., Williams, L. R., Davidovits, P., and Worsnop, D. R. Soot particle aerosol mass spectrometer: Development, validation, and initial application. Aerosol Sci. Tech., 46, 804-817, http://dx.doi.org/10.1080/02786826.2012.663948, 2012.

Ou, Y., Nie, D., Chen, H., Ye, Z., Ge, X.: Characterization of products from the aqueous-phase photochemical oxidation of benzene-diols. Atmosphere, 12, 534, https://doi.org/10.3390/atmos12050534, 2021.

Pan, Y., Ma, H., Li, Z., Du, Y., Liu, Y., Yang, J., and Li, G.: Selective conversion of lignin model veratryl alcohol by photosynthetic pigment via photo-generated reactive oxygen species, Chem. Eng. J., 393, 124772, https://doi.org/10.1016/j.cej.2020.124772, 2020.

Raja, P., Bozzi, A., Mansilla, H., and Kiwi, J.: Evidence for superoxide-radical anion, singlet oxygen and OH-radical intervention during the degradation of the lignin model compound (3-methoxy-4-hydroxyphenylmethylcarbinol), J. Photochem. Photobiol. Chem., 169, 271-278,

https://doi.org/10.1016/j.jphotochem.2004.07.009, 2005.

Richards-Henderson, N. K., Hansel, A. K., Valsaraj, K. T., and Anastasio, C. Aqueous oxidation of green leaf volatiles by hydroxyl radical as a source of SOA: Kinetics and SOA yields, Atmos. Environ., 95, 105-112, http://dx.doi.org/10.1016/j.atmosenv.2014.06.026, 2014.

Rossignol, S., Aregahegn, K. Z., Tinel, L., Fine, L., Nozière, B., and George, C.: Glyoxal induced atmospheric photosensitized chemistry leading to organic aerosol growth, Environ. Sci. Technol., 48, 3218-3227, https://doi.org/10.1021/es405581g, 2014.

Scharko, N. K., Berke, A. E., and Raff, J. D.: Release of nitrous acid and nitrogen dioxide from nitrate photolysis in acidic aqueous solutions, Environ. Sci. Technol., 48, 11991-2001, https://doi.org/10.1021/es503088x, 2014.

Schauer, J. J., Kleeman, M. J., Cass, G. R., and Simoneit, B. R.: Measurement of emissions from air pollution sources. 3. C1-C29 organic compounds from fireplace combustion of wood, Environ. Sci. Technol., 35, 1716-1728, https://doi.org/10.1021/es001331e, 2001.

Simpson, C.D., Paulsen, M., Dills, R. L., Liu, L.-J.S., and Kalman, A.A. Determination of methoxyphenols in ambient atmospheric particulate matter: Tracers for wood combustion, Environ. Sci. Technol., 39, 631-637, https://doi.org/10.1021/es0486871, 2005.

Smith, J. D., Kinney, H., and Anastasio, C.: Aqueous benzene-diols react with an organic triplet excited state and hydroxyl radical to form secondary organic aerosol. Phys. Chem. Chem. Phys., 17, 10227, https://doi.10.1039/c4cp06095d, 2015.

Smith, J. D., Kinney, H, and Anastasio, C.: Phenolic carbonyls undergo rapid aqueous photodegradation to form low-volatility, light-absorbing products, Atmos. Environ., 126, 36-44, https://doi.org/10.1016/j.atmosenv.2015.11.035, 2016.

Smith, J. D., Sio, V., Yu, L., Zhang, Q., and Anastasio, C.: Secondary organic aerosol production from aqueous reactions of atmospheric phenols with an organic triplet excited state, Environ. Sci. Technol., 48, 1049-1057, https://doi.org/10.1021/es4045715, 2014.

Stephen E. Stein (2014), NIST/EPA/NIH Mass Spectral Library with Search Program - SRD 1a, National Institute of Standards and Technology, https://doi.org/10.18434/T4H594 (Accessed 2022-04-29)

Sun, Y., Zhang, Q., Anastasio, C., and Sun, J.: Insights into secondary organic aerosol formed via aqueous-phase reactions of phenolic compounds based on high resolution mass spectrometry, Atmos. Chem. Phys., 10, 4809–4822, https://doi.org/10.5194/acp-10-4809-2010, 2010.

1167 Tang, S., Li, F., Tsona, N.T., Lu, C., Wang, X., and Du, L.: Aqueous-phase photooxidation of vanillic

1168   acid: a potential source of humic-like substances (HULIS), ACS Earth Space Chem., 4, 862-

1169   872, https://doi.org/10.1021/acsearthspacechem.0c00070, 2020.

1170 Tsui, W. G., and McNeill, V. F. Modeling secondary organic aerosol production from photosensitized

1171   humic-like   substances   (HULIS),   Environ.   Sci.   Technol.   Lett.,   5,   255-259.

1172   https://doi.org/10.1021/acs.estlett.8b00101, 2018.

1173 Verma, V., Fang, T., Xu, L., Peltier, R. E., Russell, A. G., Ng, N. L., and Weber, R. J.: Organic aerosols

1174   associated with the generation of reactive oxygen species (ROS) by water-soluble $PM_{2.5}$,

1175   Environ. Sci. Technol., 49, 4646-56, https://doi.org/10.1021/es505577w, 2015a.

1176 Verma, V., Wang, Y., El-Afifi, R., Fang, T., Rowland, J., Russell, A.G., and Weber, R. J.: Fractionating

1177   ambient humic-like substances (HULIS) for their reactive oxygen species activity-assessing the

1178   importance   of   quinones   and   atmospheric   aging,   Atmos.   Environ.,   120,   351-359,

1179   https://doi.org/10.1016/j.atmosenv.2015.09.010, 2015b.2015.

1180 Vione, D., Albinet, A., Barsotti, F., Mekic, M., Jiang, B., Minero, C., Brigante, M., and Gligorovski, S.:

1181   Formation of substances with humic-like fluorescence properties, upon photoinduced

1182   oligomerization of typical phenolic compounds emitted by biomass burning, Atmos. Environ.,

1183   206, 197-207, https://doi.org/10.1016/j.atmosenv.2019.03.005, 2019.

1184 Vione, D., Maurino, V., Minero, C., Pelizzetti, E., Harrison, M. A., Olariu, R. I., and Arsene, C.:

1185   Photochemical reactions in the tropospheric aqueous phase and on particulate matter, Chem.

1186   Soc. Rev., 35, 441-53, https://doi.org/10.1039/b510796m, 2006.

1187 Vione, D., Maurino, V., and Minero, C.: Photosensitised humic-like substances (HULIS) formation

1188   processes of atmospheric significance: a review, Environ. Sci. Pollut. Res., 21, 11614-11622,

1189   https://doi.org/10.1007/s11356-013-2319-0, 2014.

1190 Wang, J., and Wang, S. Reactive species in advanced oxidation processes: Formation, identification and

1191   reaction mechanism, Chem. Eng.J., 401, 126158, https://doi.org/10.1016/j.cej.2020.126158,

1192   2020.

1193 Wang, J., Ye, J., Zhang, Q., Zhao, J., Wu, Y., Li, J., Liu, D., Li, W., Zhang, Y., Wu, C., Xie, C., Qin, Y.,

1194   Lei, Y., Huang, X., Guo, J., Liu, P., Fu, P., Li, Y., Lee, H. C., Choi, H., Zhang, J., Liao, H., Chen,

1195   M., Sun, Y., Ge, X., Martin, S. T., and Jacob, D .J.: Aqueous production of secondary organic

1196   aerosol from fossil-fuel emissions in winter Beijing haze. Proc. Natl. Acad. Sci. USA., 118,

e2022179118, https://doi.org/10.1073/pnas.2022179118, 2021.

Wang, L., Lan, X., Peng, W., and Wang, Z.: Uncertainty and misinterpretation over identification, quantification and transformation of reactive species generated in catalytic oxidation processes: A review, J Hazard. Mater., 408, 124436, https://doi.org/10.1016/j.jhazmat.2020.124436, 2021.

Xu, X., Lu, X., Li, X., Liu, Y., Wang, X., Chen, H., Chen, J., Yang, X., Fu, T., Zhao, Q., and Fu, Q. ROS-generation potential of Humic-like substances (HULIS) in ambient $PM_{2.5}$ in urban Shanghai: Association with HULIS concentration and light absorbance, Chemosphere, 256, 127050, https://doi.org/10.1016/j.chemosphere.2020.127050 0045-6535, 2020.

Yang, J., Au, W. C., Law, H., Lam, C. H., and Nah, T.: Formation and evolution of brown carbon during aqueous-phase nitrate-mediated photooxidation of guaiacol and 5-nitroguaiacol, Atmos. Environ., 254, 118401, https://doi.org/10.1016/j.atmosenv.2021.118401, 2021.

Ye, Z., Zhuang, Y., Chen, Y., Zhao, Z., Ma, S., Huang, H., Chen, Y., and Ge, X.: Aqueous-phase oxidation of three phenolic compounds by hydroxyl radical: Insight into secondary organic aerosol formation yields, mechanisms, products and optical properties, Atmos. Environ., 223, 117240, https://doi.org/10.1016/j.atmosenv.2019.117240, 2020.

Yu, L., Smith, J., Laskin, A., Anastasio, C., Laskin, J., and Zhang, Q.: Chemical characterization of SOA formed from aqueous-phase reactions of phenols with the triplet excited state of carbonyl and hydroxyl radical, Atmos. Chem. Phys., 14, 13801–13816, https://doi.org/10.5194/acp-14-13801-2014, 2014.

Yu, L., Smith, J., Laskin, A., George, K. M., Anastasio, C., Laskin, J., Dillner, A. M., and Zhang, Q.: Molecular transformations of phenolic SOA during photochemical aging in the aqueous phase: competition among oligomerization, functionalization, and fragmentation, Atmos. Chem. Phys., 16, 4511-4527, https://doi.org/10.5194/acp-16-4511-2016, 2016.

Zhang, T., Huang, S., Wang, D., Sun, J., Zhang, Q., Xu, H., Ho, S., Cao, J., and Shen, Z. Seasonal and diurnal variation of $PM_{2.5}$ HULIS over Xi'an in Northwest China: Optical properties, chemical functional group, and relationship with reactive oxygen species (ROS), Atmos. Environ., 268, 118782, https://doi.org/10.1016/j.atmosenv.2021.118782, 2022.

Zhang, X., Chen, Z. M., and Zhao, Y.: Laboratory simulation for the aqueous OH-oxidation of methyl vinyl ketone and methacrolein: significance to the in-cloud SOA production, Atmos. Chem. Phys., 10, 9551-9561, https://doi.org/10.5194/acp-10-9551-2010, 2010.

1227 Zhao, R., Lee, A. K., and Abbatt, J. P.: Investigation of aqueous-phase photooxidation of glyoxal and
1228   methylglyoxal by aerosol chemical ionization mass spectrometry: observation of
1229   hydroxyhydroperoxide formation, J. Phys. Chem. A., 116, 6253-63,
1230   https://doi.org/10.1021/jp211528d, 2012.

1231 Zhao, R., Mungall, E. L., Lee, A. K. Y., Aljawhary, D., and Abbatt, J. P. D.: Aqueous-phase
1232   photooxidation of levoglucosan-a mechanistic study using aerosol time of flight chemical
1233   ionization mass spectrometry (Aerosol ToF-CIMS), Atmos. Chem. Phys., 14, 9695-9706,
1234   https://doi.org/10.5194/acpd-14-8819-2014, 2014.

1235 Zhao, R., Lee, A.K.Y., Huang, L., Li, X., Yang, F., and Abbat, J.P.D.Photochemical processing of aqueous
1236   atmospheric brown carbon, Atmos. Chem. Phys., 15, 6087-6100, https://doi.org/10.5194/acpd-
1237   15-2957-2015, 2015.

1238 Zhou, Z., Chen, B., Qu, X., Fu, H., and Zhu, D.: Dissolved black carbon as an efficient sensitizer in the
1239   photochemical transformation of 17#-β-estradiol in aqueous solution, Environ. Sci. Technol.,
1240   52, 10391-10399, https://doi.org/10.1021/acs.est.8b01928, 2018.